RICE UNIVERSITY

ELECTRON PARAMAGNETIC RESONANCE OF EXCITED SPECIES CREATED BY ELECTRON BOMBARDMENT

by

Edgar Durbin Jr.

A THESIS SUBMITTED
IN PARTIAL FULFILLMENT OF THE
REQUIREMENTS FOR THE DEGREE OF

DOCTOR OF PHILOSOPHY

Thesis Director's signature:

Houston, Texas

September, 1971

Table of Contents

Figures

Chapter I

Introduction

This thesis reports part of a series of investigations conducted since 1963 in the Atomic Physics Laboratory at Rice University into excited species in gaseous and liquid helium. The complex set of physical processes present in such systems have been studied in experiments in optical pumping, polarized beams and targets, spin conservation in collisions, and diffusion constants of metastable atoms. The reactions which predominate are determined in part by the density of the system, a fact which made desirable an extension of early work in low pressure gas into studies of high density gas and liquid. These experiments required the development of a new method for creating excited species, since continuous radio frequency discharges, used in previous work, cannot be maintained in room temperature gas above about 100 Torr ($10^{19}cm^{-3}$). Such a technique was developed in this laboratory, using a 200 keV electron accelerator separated by a thin foil from a high density target gas (up to $10^{21}cm^{-3}$) or liquid ($10^{22}cm^{-3}$).

While providing an intense excitation source in high density gas and liquid, the accelerator has the additional advantage of permitting the measurement of excited state lifetimes and decay modes when the beam is pulsed. The range of conditions

under which excited helium species might be studied was further extended by fitting the sample chamber in a Dewar, providing temperature control of the sample from 1.5°K to room temperature.

As well as extending previous gas-phase helium studies to higher densities, the accelerator-Dewar arrangement permitted investigation of an effect reported by Jortner et al[1] in liquid helium excited by a ^{210}Po α-source. Energy absorbed by the helium in stopping the α-particles was emitted not as a helium spectrum, but as a spectrum of molecular nitrogen and oxygen, species present in very dilute solution or colloidal suspension in the helium. To investigate the mechanism by which energy was transferred to the relatively rare impurity atoms, an extensive study was made at Rice of the emission spectrum of electron-bombarded liquid and gaseous helium (1967-1969)[2,3,4,5]. In this work, the shifts of spectral features with density and the rotational and vibrational temperatures of molecular helium yielded interesting theoretical models of the environment in which an excited helium atom or molecule exists in superfluid helium. At the same time that these models were being tested by absorption spectroscopy in the visible and near IR, work started on a new apparatus, with which we might observe electron paramagnetic resonance (EPR) of excited metastable helium states. Since magnetic transitions are at microwave frequencies, (10^{10}Hz) in a 3kG field, while the electronic transitions associated with emission and absorption

spectroscopy are at optical frequencies (10^{15}Hz), it was hoped that the small interaction energies of the excited electrons with other electrons and nuclei would have proportionately greater effect on the EPR spectrum. Thus the environment in which the excited helium atoms exist might be studied more closely with EPR. This thesis describes the design and use of the apparatus built for this purpose. Construction details and performance characteristics are contained in Chapter II.

The first system to which the complete accelerator-Dewar-spectrometer was applied was superfluid helium, but no EPR signal was detected. Concurrent experiments in optical absorption spectroscopy of electron-bombarded liquid helium measured a density of metastable helium atoms and molecules too small for the EPR spectrometer to have detected[6]. A further impediment to observing EPR was the anticipated long spin relaxation time of 2^3S atoms in liquid ^{4}He, discussed in Chapter III. While plans were made to increase the sensitivity of the spectrometer and to decrease the relaxation time of helium, an attempt was made to detect an EPR signal in another substance.

The hydrogen atoms produced by bombardment of solid hydrogen at 4.2°K provided the first EPR signal detected with our apparatus. The spectrum we recorded was reported by Piette et al[7] in 1959 and is discussed in Chapter IV. We detected no EPR in liquid hydrogen, probably because the recombination rate

of hydrogen atoms in the liquid is too high to permit a detectable density to accumulate.

We were introduced to another class of experiments to which our apparatus is suited by Robert J. Shalek of M. D. Anderson Hospital and Tumor Institute at Houston. He suggested that irradiated proteins might serve as model systems with which to investigate radiation damage in living organisms and radiation therapy of human cancer and that EPR might provide detailed information on the reactions involving radicals formed by ionizing radiation in such simple systems. Accordingly, the apparatus was adapted to aqueous samples, which have a high electric loss factor.

An EPR signal was detected in irradiated powdered lysozyme. This enzyme was chosen so that our work would complement studies of lysozyme made by Shalek and others. Our efforts to find a signal in lysozyme-water solutions and the significance of experiments on this substance are described in Chapter V.

Chapter II

Apparatus

Our apparatus consists of three major components, which we shall describe in this chapter. The accelerator will be considered first, starting at the source of the electrons and moving in the direction of the beam until it leaves the drift tube and enters the second component, the Dewar. The feature of this device with which we shall be principally concerned is the foil, separating the vacuum of the accelerator from the samples cooled by the Dewar. These are contained in the cavity at one end of the third component, the microwave spectrometer. Some of the features of this instrument will be described and the limitations on its sensitivity will be covered at the end of the chapter.

A. Accelerator

The principal features of the accelerator are seen in Figure 1, p. 6. The horizontal steel frame supports a vertical plate of 1" thick aluminum, on one side of which hangs the corona shield and terminal, the accelerating column, and the resistor stack.

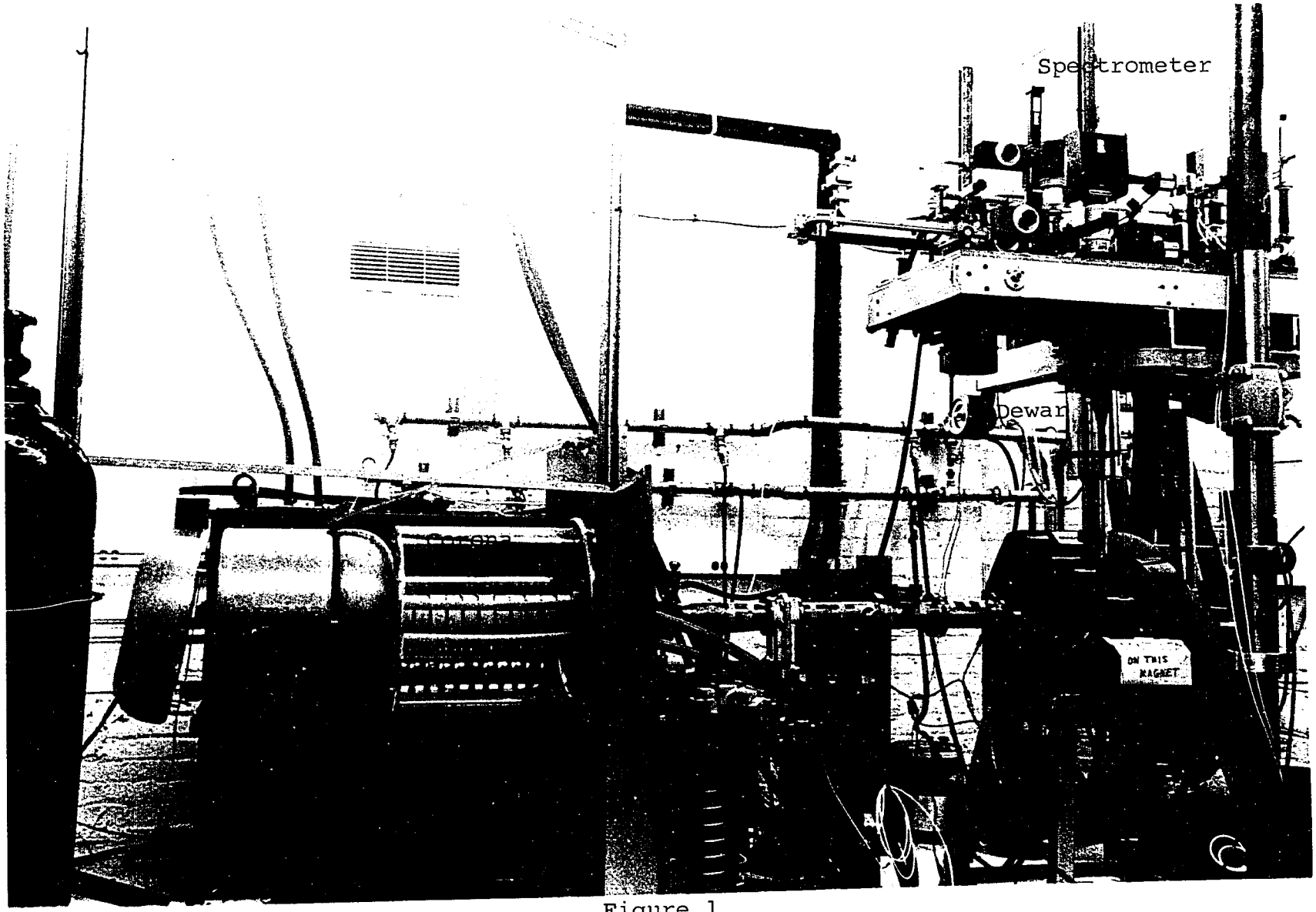

Figure 1
Accelerator, Dewar, and microwave spectrometer

The accelerating voltage is supplied by a 200kV 5mA Universal Voltronics BAL-200-55R2 power supply. One lead from this supply maintains the spun aluminum terminal at the head of the accelerator at up to -200kV, and another lead, at HV + 110 Vac, passes through a hole in the terminal and powers the cooling fan, grid pulser, and extractor power supply, which are housed inside the terminal. The terminal is grounded through twenty 10 megohm resisters in series. The accelerating column, manufactured by Texas Nuclear Corporation, consists of a flange which mates with the electron gun, a flange at ground, and in between, ten accelerating electrodes separated by ceramic insulators. (See Figure 2, p. 8.) The electrode closest to the terminal makes contact inside the column with the extractor of the electron gun, and on the outside it is connected to the 10kV extractor power supply housed in the terminal. The next nine electrodes tap off the 200 megohm resistor stack at 20 megohm intervals. In our experiments, the extractor power supply was set at 5kV and the terminal at 160kV.

The electron gun was designed by K. H. Steigerwald for use in electron microscopy[8,9]. Considerable experimentation was necessary before we learned proper adjustment of this gun to obtain a sharp, steerable beam of electrons after acceleration and focussing. The most critical element is the grid, which must be sufficiently negative with respect to the filament to

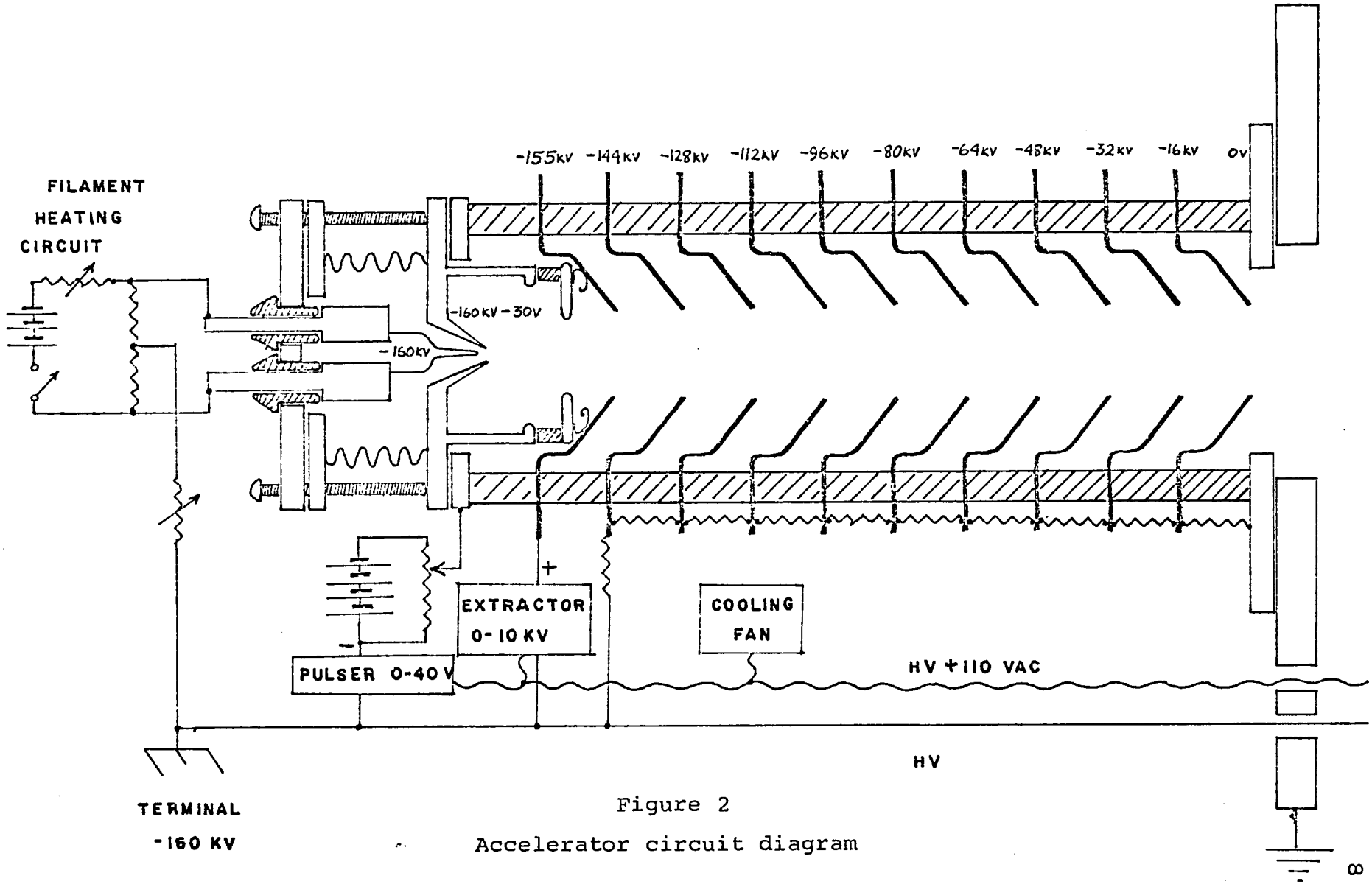

Figure 2

Accelerator circuit diagram

lead to a narrow beam emerging from the accelerating column, but not so negative that filament emission is suppressed. It seems likely that the grid voltage not only focusses the electrons that escape the filament and are extracted, but also prevents the entry of electrons into the grid-extractor space that are emitted from the filament at large angles to the accelerating column axis. With insufficient grid voltage, the latter electrons might charge up exposed insulator in the electron gun, causing the main beam to be deflected. To set the grid potential, auto-biasing was first tried. This involves a circuit in which the current of electrons flowing from the terminal to replace electrons boiled off the filament passes through a variable resistor.[10] Assuming a constant current, if the grid is at the terminal potential, it will be negative with respect to the filament in proportion to the size of this resistor. This method of grid biassing did not work, since the current was not constant, but varied inversely with the resistor. A successful method of biassing the grid is shown in Figure 2. When turned off, the General Radio pulser is shorted out and the grid is biassed at a constant value, typically 30 volts. Turned on, the pulser generates pulses of up to 40 volts, which cut off filament omission. Beam pulses at 1 kHz and variable duration with a time constant of less than 50μsec have been measured at the output of the accelerator.

The beam current is controlled by the filament

current, the grid potential, and the resistor between the filament and the terminal. This last control has least effect and was rarely moved from its setting at minimum resistance (about 10 ohms). The filament current was usually 5 to 6A and was not often adjusted. By adjusting the grid potential, the beam current can be varied over several orders of magnitude (10nA to 10μA) without much affecting the focussing of the beam, and we usually used this control to set beam current.

The filament is a piece of .012" tungsten wire about 1 1/2" long and bent to a fairly sharp point (about 1/32" radius) in the middle, so that it can be extended as far as possible into the conical grid. The tip of our filament is about 1/32" from the 1/32" hole in the grid, as far as it can be advanced without touching the side of the grid. With 5 to 6A flowing through it, this filament glows yellow-orange and has a resistance of about .23 ohms. The filament current is driven by three Yardney 40A-hr silver cells of total voltage about 4.5V.

Adjustments of equipment inside the terminal can be made while the high voltage is on with yard-long 1/2" Plexiglas rods extending through holes in the rear cover of the terminal. Controls include filament on/off, filament current, resistance between the filament and the terminal, grid bias, pulse repetition frequency coarse and fine, pulse duration coarse and fine, pulse amplitude, and extraction voltage coarse and fine. With

the high voltage off, the rear terminal cover can be snapped off the terminal and slid back, along the control rods, to permit direct adjustment of terminal components.

The terminal is supported by a cylindrical Plexiglas corona shield 17" in diameter surrounding the accelerating column and resistor stack from the ground flange to the electron gun. The gap between the electron gun and the corona shield is bridged by an annulus of flexible .010" plastic, so that the volume between the accelerating column and the corona shield is airtight except for a couple of small feed-through holes for cables from the terminal to the extractor electrode and to the end of the resistor bank. This space is flushed occasionally with dry nitrogen to prevent corona discharge between the accelerating electrodes.

The drift tube is bolted to the other side of the ground plate. The first section of drift tube contains the deflection plates and is circled by a water-cooled coil that focusses the beam about 5 feet away. (See Figure 3, p.12.) As well as affecting the cross section of the beam, this coil deflected the beam, though it was roughly concentric and parallel with the drift tube. Equal and opposite voltages are applied to the deflection plates, typically ±500V. An aperture confines the beam to the area between the deflection plates and restricts the number of secondary electrons entering

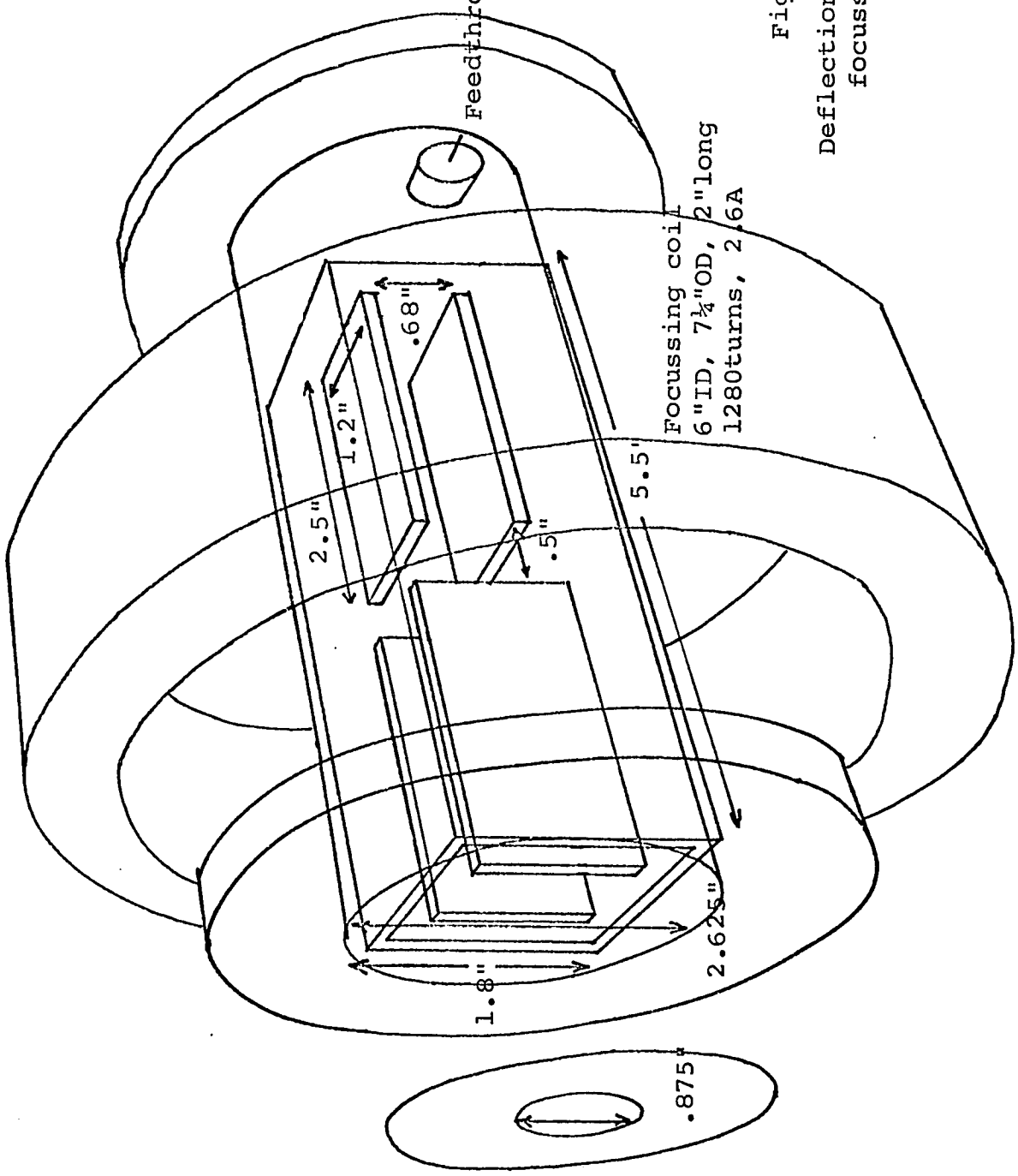

Figure 3
Deflection plates and
focussing coil

the drift tube.

The next section of drift tube is a pumping T. Coming off the pumping arm of this T are a 4" gate valve, a cold cathode vacuum gauge, a 6" TriMetal diffusion pump, and a forepump. The exit of the pumping T is connected to a 2" pneumatic valve. The compressed air powering this valve is switched by solenoids controlled either manually or by a safety system. The cold cathode gauge is connected to the safety system through a National Research Company model 889 controller. When this gauge measures a pressure as high as 10^{-4} Torr, the pneumatic valve is closed to isolate the Dewar from the accelerator and to prevent a possible leak through the foil from damaging the hot filament or the diffusion pump. If the pressure continues to rise to 10^{-3} Torr, due to a leak somewhere in the accelerator, the diffusion pump is shut off.

Following the pneumatic valve is the third section of drift tube. It has two 1 3/4" flanges, to which are connected a 3/8" valve, for roughing and bleeding, and a thermocouple gauge. A crutch from the accelerator frame supports this section, so that the entire drift tube and diffusion pump are held up by this crutch and by the vertical ground plane, to which the first section is fastened.

The next section is a T with a Plexiglas window blanking off the middle arm and a small piece of CRT screen, which can be moved into or out of the electron beam. With mirrors

and a telescope it is possible to see through the window the cross section of the beam striking the CRT screen, while adjusting the focussing and deflection controls.

The fifth section of drift tube is insulated from the viewing T by a 1" piece of Plexiglas. As with all preceding sections of the drift tube, this section has a 2.6"ID; but the exit flange has only a 3/8" hole, through which the beam must be steered. It is also insulated from the following, and last, piece of drift tube by 1" of Plexiglas. Thus, an ammeter connected to the fifth section can be used while steering the beam into the sixth section, which is .425"ID. The earth's magnetic field in our lab curves the electron beam enough to make it impossible to steer the beam into the sixth section unless the fifth section is wrapped with conetic magnetic shield. A further improvement in beam was obtained by shielding the viewing T, and for good measure the third and second sections were shielded, too.

The sixth section of drift tube narrows to 1/2"OD in order to pass through an axial hole in the magnet and reach the Dewar. Details of this section are seen in Figure 4, p. 15 This section is electrically insulated from the preceding section, from the magnet, and from the Dewar, in order to make it possible to measure beam current.

A closed cooling system, connected to the diffusion pump, the beam focussing coil, the magnet, and the helium pump, is used to avoid corroding these devices with tap water. A

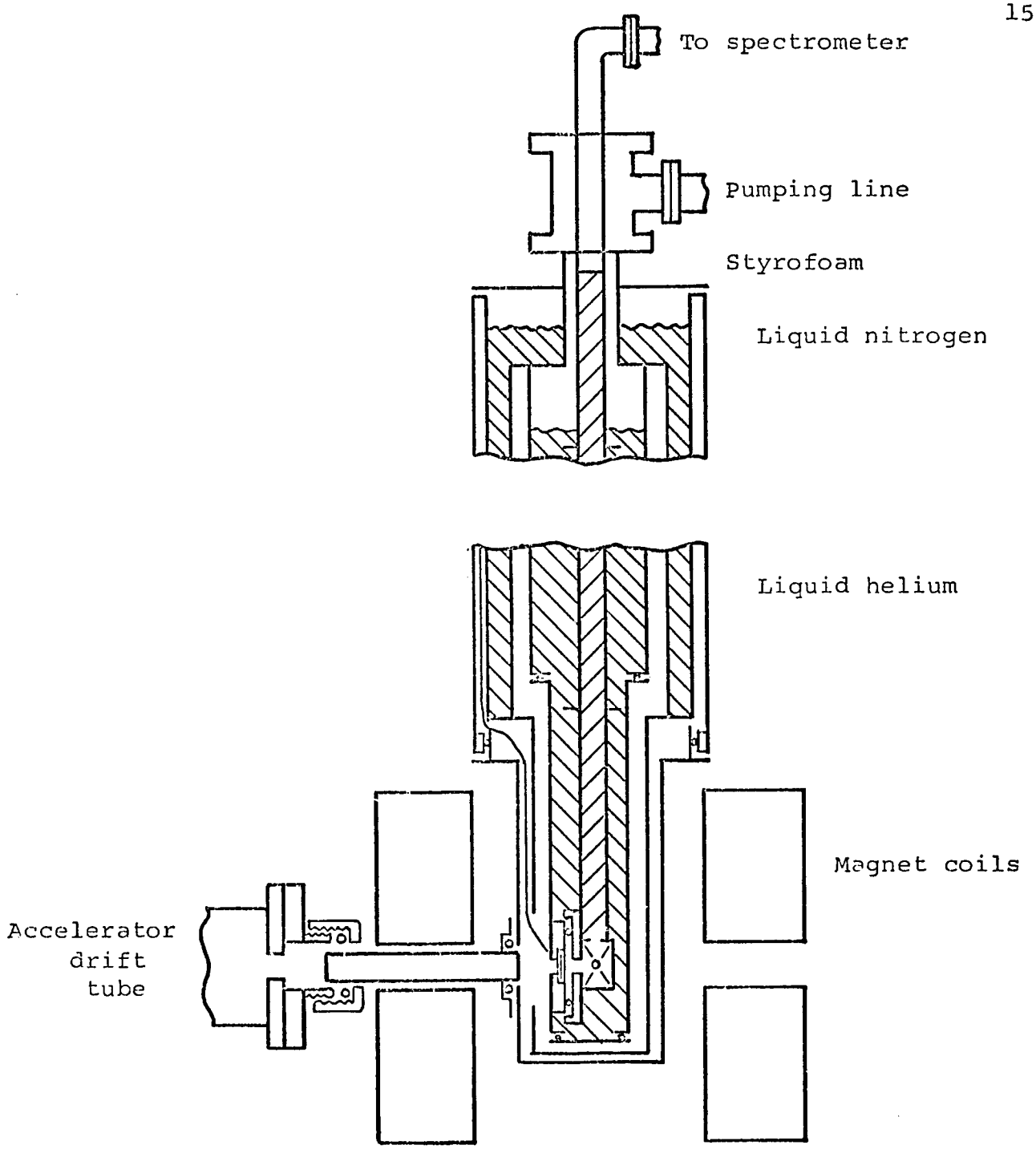

FIGURE 4

DEWAR, BEAM TUBE, MAGNET, & CAVITY

See also Figure 5 for close-up of cavity

pressure switch in the line to the diffusion pump will detect a fall in water pressure (due to a line break or pump failure, for example) and cause the safety system to shut off the water pump and diffusion pump and to close the pneumatic valve. A bimetallic switch in thermal contact with the cooling water leaving the diffusion pump will detect a rise in temperature of the pump and cause it to be turned off.

B. Dewar

The second major element in the apparatus is the stainless steel Dewar. The body of this Dewar is a Janis Research Company model 2D-2L. The outermost tail is vacuum sealed to the 1/2"OD sixth section of drift tube, and contains 1" sapphire windows at 90°, 180°, and 270° to the drift tube. (These windows were designed for the earlier study of the emission and absorption spectrum of electron-bombarded liquid helium, mentioned in Chapters I and III.) The accelerator vacuum pumps evacuate the Dewar through the 1/2" drift tube. The inner tail has a 3/8" hole through which the electron beam enters, and windows at 90°, 180°, and 270° to the beam that line up with holes in the radiation shield and the windows in the outer tail. (See Figure 5, p. 17) A microwave cavity, which fits inside the inner cavity, covers the 3/8" hole and permits the inner tail to be filled with liquid helium. An indium O-ring crushed between the cavity and the inner tail prevents liquid helium from

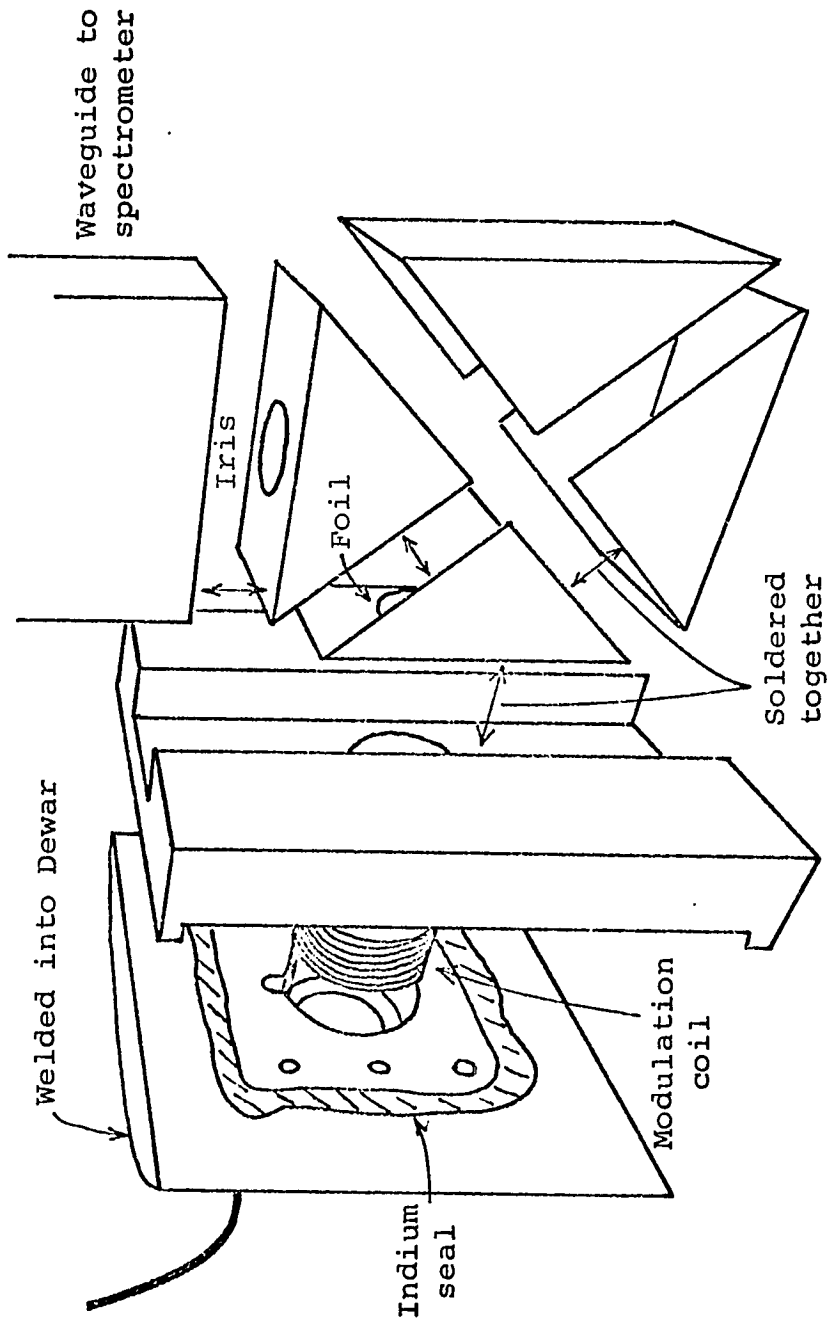

Figure 5

Cavity, modulation coil, and Dewar

leaking out of the inner tail through the 3/8" hole. A .000125" thick Havar foil soldered into one wall of the cavity faces the 3/8" hole. The electron beam emerges from the 1/2"OD drift tube, passes through a hole in the radiation shield, the 3/8" hole in the inner tail, and the thin foil, to strike the sample inside the cavity.

Theoretical calculations predict that a 160keV electron beam will only lose about 10% of its energy in passage through the foil. Variation in energy of the transmitted electrons will be about ±1% from the average energy.[3] The extrapolated range of 160keV electrons is 29.4 mg/cm^2 and the thickness of the foil is 2.64 mg/cm^2, so the beam will be stopped in only 26.8 mg/cm^2 of sample, which is .176 cm of liquid helium or .0268 cm of water.

Our apparatus thus has the advantage of very thin samples close to the cavity wall, where the microwave magnetic field is maximized and the electric field is minimized. This arrangement minimizes dielectric losses in samples with electric dipole moments, such as water or water solutions.

Experiments conducted early in development of the beam-foil technique in this lab showed that this foil can withstand 300μA of beam current without being damaged.[2] A much lower limit to beam current is set by the sample, as discussed in Chapter III for liquid helium, Chapter IV for hydrogen, and

Chapter V for water solutions.

Since the conductivity of the Havar foil is less than copper (1.1×10^6 mho/m v.s. 58×10^6 mho/m) the foil reduces the Q of the cavity from about 3000 to 2300.

Though the foil is taut under the atmosphere pressure inside the cavity when the beam tube is evacuated, in some circumstances it can jitter enough to cause appreciable microwave noise. The necessary conditions are a large modulation field to cause eddy currents to flow in the foil, a 3kG static field to exert a force on the eddy currents, and a dry or powdered sample, which may be pushed away from the foil and not damp the jittering.

The temperature of the helium in the inner tail is controlled by a model KDH-65 Kinney vacuum pump and a pumping flow regulator. This pumping arrangement maintains the helium at any temperature between 4.2°K and 1.5°K. Other liquids used to fill the inner tail give higher sample temperatures.

The Dewar is supported by a 3 1/8"OD steel post extending from ceiling to floor. A Rockwell model 17-825 drill press table is mounted on this post, and may be moved 3' vertically by a Rockwell model 17-801 raising mechanism, consisting of a worm gear, reduction gear, and rack. The Dewar rests on two horizontal aluminum L-beams bolted to the table, and may be moved vertically in or out of the magnet gap. Since the rack

rests on a thrust bearing, it and the table and Dewar may be rotated around the post, when the Dewar is raised out of the gap, to move the Dewar away from the magnet for servicing.

C. Spectrometer

The third element of our apparatus is the microwave spectrometer, which sits on a wooden table that is built on the drill press table, and thus moves up and down with the Dewar. A 3' length of .010" wall stainless steel X-band waveguide connects the cavity to the spectrometer and is filled with Styrofoam. Without this, the waveguide would fill with liquid helium, which would reflect microwaves with a phase which would vary with the height of the liquid, interfering with operation of the spectrometer. The waveguide passes through two small radiation shields inside the Dewar and a flange on top of the helium pumping T before joining an H-plane bend. This bend is sealed at the other end with a vacuum tight microwave window, which permits evacuation of the waveguide and prevents condensation of air into the cold waveguide and cavity.

The original cavity was designed for the TE_{101} mode, with inner dimensions .9" x .9" x .4". (See Figure 5, p. 17 The shape of the four sections of oxygen-free, high purity copper which comprise this cavity is such that no eddy currents

associated with the TE_{101} mode have to cross a junction between two sections. Thus the resistance through which the current must flow is minimized and the cavity Q is maximized. A 1/16" hole at the two points where all four sections meet permits helium from the inner tail to fill the cavity. A later cavity, lacking this hole and completely soldered together, is filled by condensing helium or other gas admitted *via* the iris and the waveguide soldered above the iris.

The magnetic field at the sample is modulated by a small coil mounted in the inner tail. The alternating magnetic field that this coil can produce at the sample seems to be limited by current loops induced in the outside of the cavity wall containing the foil. This effect is magnified at low temperatures, when the resistance of the cavity wall is reduced. Another limit to the modulation field is the maximum current the coil can carry without overheating. Unfortunately, poor thermal contact between the coil and the inner tail leaves the coil considerably warmer than the tail, so the resistance of the coil does not fall much when the Dewar is cooled to liquid helium temperatures. The screening effect of induced current loops increases faster than the maximum allowed current through the coil, so the maximum modulation field at a given frequency decreases with temperature. In order to achieve a modulation field of .3G in the cavity at 1.75°K, it is

necessary to drive the modulation coils at 40Hz with the maximum allowed current, about .6A. At room temperature, however, the same field is produced by the same current at 2000Hz.

A 10dB directional coupler between the cavity and the spectrometer permits measurement of the noise figure of the whole system from the cavity to the output of the lock-in amplifier. (See Figure 6, p. 23.) A model MC5812 29dB Microwave Semiconductor Corporation noise source was connected to the second part of the coupler, sending 19dB of excess noise out of the third port, into the rest of the spectrometer. The noise figure F of a system is defined as

$$F = \frac{S/N/in}{S/N/out} .$$

The signal-to-noise ratio at the input is that of the noise diode, less 10dB. Thus,

$$\left.\frac{S}{N}\right|_{in} = \frac{\text{(noise with diode on) - (noise with diode off)}}{\text{noise with diode off}} = 10^{1.9} .$$

The output signal-to-noise ratio is measured at the lock-in amplifier output.

$$\left.\frac{S}{N}\right|_{out} = \frac{\text{(lock-in noise with diode on) - (lock-in noise with diode off)}}{\text{lock-in noise with diode off}}$$

In the balanced homodyne spectrometer first used, it was found that when the signal arm includes 70dB or more attenuation, less power is incident on the cavity via the signal arm than via the bias arm, magic T, and circulator. In this latter

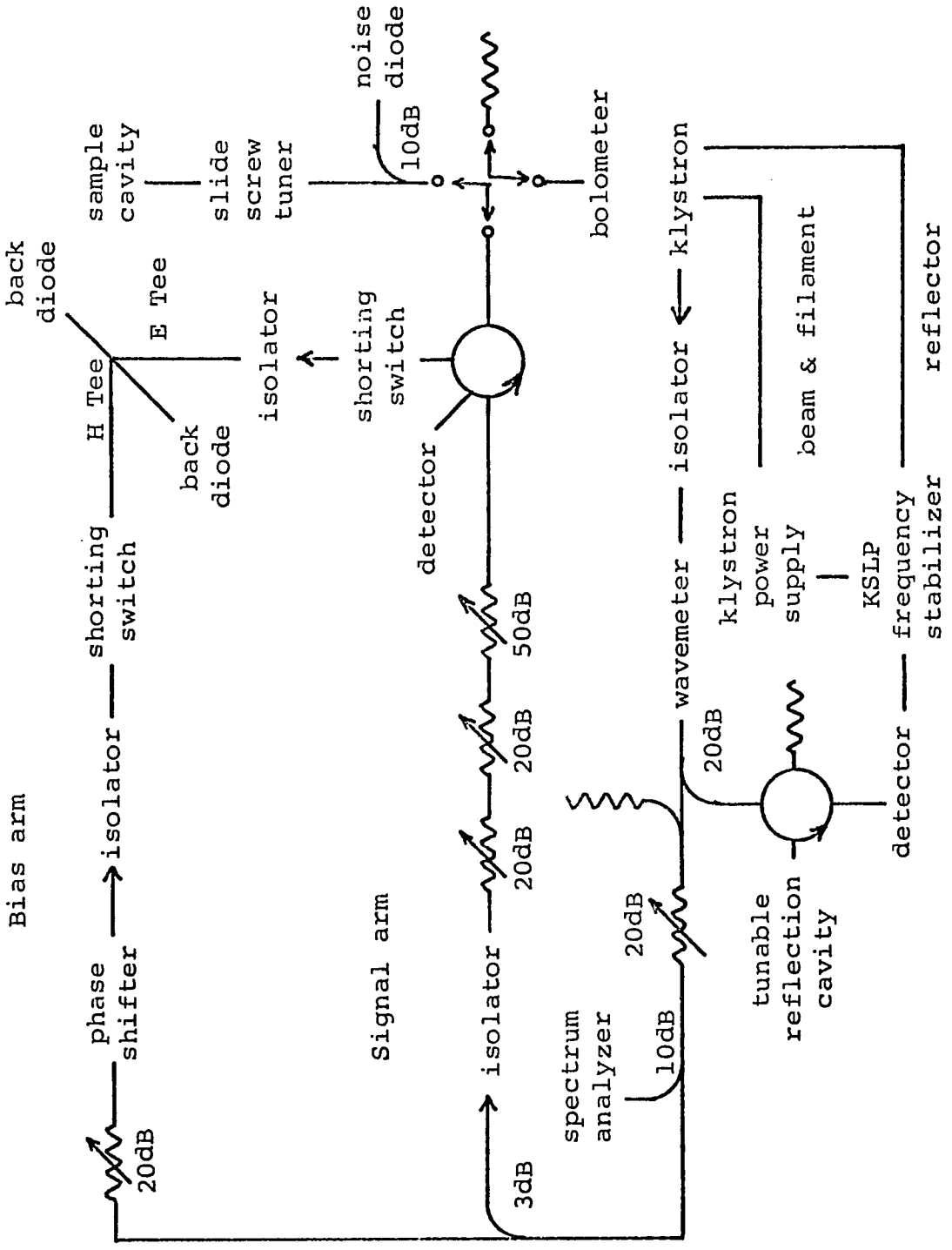

Figure 6

Spectrometer schematic

route, 1mW in the bias arm is attenuated by about 20-30dB in going from the H-plane arm to the E-plane arm of the magic T and is further attenuated by 40dB in going through the circulator backwards. Such a situation leads to a signal at the detectors which is insensitive to the phase shifter, so that we cannot tune for absorption or dispersion signals. This problem was corrected by including an isolater between the magic T and the circulator, to increase the isolation of the cavity from the bias arm by 20-40dB.

The X-13 klystron is usually locked in frequency to a deMornay-Bonardi tunable cavity, since the low powers commonly incident on the sample cavity make it inconvenient to use in the frequency stabilization circuit. A Teltronix KSLP klystron stabilizer frequency modulates the klystron microwave output at 70kHz by amplitude modulating the klystron reflector voltage. The FM microwaves are reflected from the tunable cavity and detected. If the microwave center frequency is close to the resonant frequency of the cavity, the reflection coefficient of the cavity will be strongly frequency dependent and the microwaves reflected to the detector will be amplitude modulated. The output of the detector is thus a 70kHz signal whose phase is dependent on the sign of the frequency difference between the cavity and the klystron. This signal is converted by the KSLP into a d.c. voltage impressed on the

klystron reflector such as to move the microwave center frequency to coincide with the cavity resonant frequency.

This method of frequency stabilization leads to microwave sidebands at intervals of 70kHz on either side of the center frequency, which can be clearly seen with a spectrum analyzer. By reducing the amplitude of the 70kHz reflector modulation to its minimum operable value, all sidebands can be made to vanish but the first, which are 1/5 to 1/10 the amplitude at the central frequency.

These sidebands appreciably increase the noise from the sample cavity, since with the center frequency set on the cavity resonance the sidebands are at frequencies where the reflection coefficient of the cavity is frequency dependent.

The back diodes mounted on the magic T are another source of noise. This type of crystal microwave diode was chosen for its low noise figure at low frequencies. The shielding effect of the metal cavity, mentioned above in the discussion of the modulation coils, necessitates low modulation frequencies (10Hz - 10,000Hz), a region in which back diodes have lower noise figures than other crystals. Since the noise figure in this range varies as 1/f, it is desirable to use the highest modulation frequency possible.

Because a large load resistance will bias a back diode to a point on its i-v characteristic with small gain and high noise, these diodes must be used with a preamp of very low

input resistance.[11] Diode noise will begin to increase when the load is of the order of the diode impedance, which is between 50 and 200 ohms, depending on the r.f. bias level.

The Princeton Applied Research Type B preamp meets this requirement, since it is a 1:100 transformer with a primary resistance of 2 ohms. This preamp, used with the PAR Model HR-8 lock-in amplifier, also has the appropriate frequency response, 10Hz to 10kHz. In turn, the back diodes fit the requirements of the Type B for input impedance to minimize amplifier noise figure. By connecting the diodes in parallel (see Figure 7) their impedance becomes 25-100 ohms,

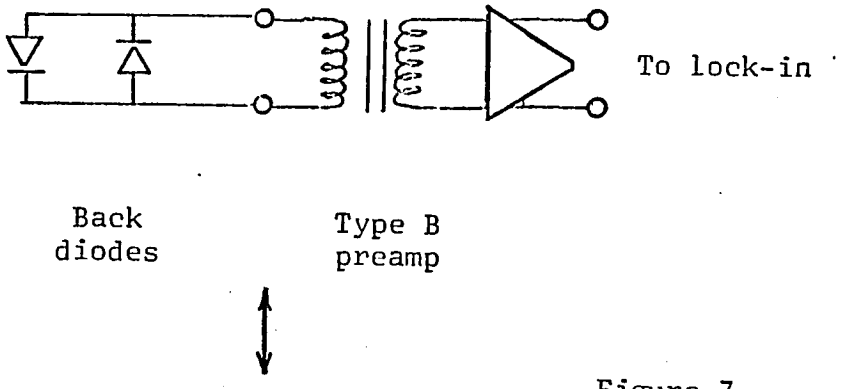

Figure 7

Back diodes and preamp

and if their polarity is opposed, the d.c. voltages resulting from the r.f. bias will tend to cancel, leaving only a very small d.c. voltage across the preamp input. This arrangement meets another requirement of the Type B, that d.c. currents should not flow through the primary, since they may permanently magnetize the transformer core and thus degrade its performance. Variations in the bias level do not show up at the preamp input, since the diodes are opposed. Thus, klystron AM noise is not transmitted through the bias.

The spectrometer was calibrated using a sample prepared and calibrated to $\pm 25\%$ by Varian Associates. The spins were on the molecules of pitch in a 1% dry mixture of pitch in KCl packed into a long, thin quartz tube. The tube extended through a small hole in the bottem of the cavity, giving a cylindrical sample close to the foil extending from the floor of the cavity to the top.

At 3×10^{15} spins/cm this put 7×10^{15} spins in the cavity. Since the ends of the sample were in the corners of the cavity, where the microwave field was reduced, it was estimated that this sample would give a signal equal to about 5×10^{15} spins concentrated at the foil. The measured sensitivity was $(1.5 \pm 1) \times 10^{13}$ spins for a room temperature sample with a 1 G line, a modulation field at 200Hz or 1000Hz with the largest amplitude possible without causing line broadening,

RC = 1 second, and 1mW power incident on the cavity. With x10 modulation field, about x1/3 this number of spins could have been detected. This agrees with the theoretical sensitivity calculated in the appendix from the measured noise figure of the system and cavity Q.

The theory of the appendix predicts that the minimum detectable number of spins N_{min} will decrease with the 3/2 power of the sample temperature. Such an increase in sensitivity is not possible, however, for several reasons. The theory assumes the existence of a constant noise figure F such that the noise power N_o out of the system of gain G is related to the input noise N_i by

$$N_o = FG\, N_i.$$

This relation is obviously not valid when noise from the cavity N_i is less than noise generated in the diodes by bias, for then N_o is independent of N_i. This consideration leads to a different relation,

$$N_o = FGN_i + \text{constant}$$

and $N_{min} \propto \sqrt{FkT_S\Delta f + \text{constant}}$. The results of the appendix are valid for powers greater than about 0.1mW since cavity noise is greater than bias noise in this region.

Another practical limit on sensitivity, not reflected by the expression for N_{min}, is the decrease in modulation field with temperature. It was assumed in calculating N_{min} that the

signal from the sample, S_i, at a frequency $f \pm 1/2\Delta f$, was the difference in power reflected by the cavity off-resonance and on-resonance. That is, modulation was assumed sufficient to sweep the sample from the center of the EPR absorption line to the wings. If the sample temperature is lowered, reducing $N_{min} \propto T_e\sqrt{FT_s + \text{constant}}$, to meet the condition of full modulation implicit in this equation, the modulation frequency must be lowered, which causes F to rise. An indefinite improvement in sensitivity is not possible by lowering the sample temperature, therefore.

Chapter III

Liquid Helium

The experiment for which the apparatus described in Chapter II was designed was the search for EPR of metastable atomic and molecular species in superfluid helium. Preceding the design of this apparatus we had studied the optical emission spectrum of electron-bombarded liquid helium for more than a year, using a commercial accelerator. It was first determined that a beam of up to .3mA at 160keV from this older machine could be passed through a Havar foil to excite a gaseous sample at 1 atmosphere without damaging the foil.[2] It was then found that excitations in superfluid liquid helium could be produced by electron bombardment without causing the liquid to boil, if the beam current was less than 30 A.[5] These preliminary investigations were followed by a series of experiments to record the visible and near infrared spectrum emitted by liquid excitations.

In place of the microwave cavity described above, a sample chamber was fit into the Dewar, with a foil to admit the electron beam and sapphire windows at 90° and 270° to the beam to transmit light emitted by the excitations. The inner tail was filled with liquid helium transferred from a storage Dewar, cooling the evacuated sample chamber to 4.2°K. By

admitting slightly more than an atmosphere of helium gas to the chamber, pure liquid helium could be condensed without contamination from atmospheric gases. Temperatures as low as 1.5°K could be achieved by pumping away the helium vapors above the coolant bath.

Identification of the excited species emitting the liquid spectrum was made by comparing liquid spectra to spectra of dense gases recorded with the same apparatus.[3] Rotational lines, resolved in gas spectra but not in the liquid, yielded molecular constants that were compared with values reported in the literature to identify the atomic and molecular states involved in the observed transitions.

Liquid transition wavelengths could then be compared to the corresponding low pressure gas wavelengths to determine the shift due to liquid interactions. The shifts in wavelength were much smaller than one would expect in the liquid where the average interatomic distance is smaller than the diameter of an excited state. The small shifts could be explained only by assuming that ground state helium atoms were excluded from a region surrounding the excited species, reducing the interaction of these species with the liquid. Theoretical calculations of liquid-excited state interactions predict a bubble of radius about 10 Bohr radii surrounding the 2^3S metastable atom.[4,12] Bubbles of similar size can be

expected to stabilize excited molecular states in liquid helium.

To further study the local environment in which excitations exist in liquid helium, the present apparatus was built. The first objective was the detection of EPR of electrons in the 2^3S atomic state and the $a^3\Sigma_u^+$ molecular state, species which were expected to be metastable because their decay is spin-forbidden. A literature search found no account of the EPR spectrum of excited states of helium.[13,14,15] Our attempt to detect EPR in liquid ^4He bombarded by electrons failed, probably because too few metastable electrons were produced and because their spins did not relax fast enough.

About the time of our first EPR experiments, an optical absorption experiment was performed by Heyboy, Hill, and Walters, using the original commercial accelerator and another Dewar.[6] They found about 5×10^{11} helium molecules in the metastable $a^3\Sigma_u^+$ state of He_2 and 5×10^{10} atoms in the metastable 2^3S atomic state in liquid helium excited by a $1\mu A$ beam. Though the 2^3S density was linear in beam current, the $a^3\Sigma_u^+$ density increased only as the square root of beam current. No more than about 3×10^{12} excitations could be created in steady state, therefore, without boiling the liquid with the beam. This is only a factor of 2 fewer than

the minimum detectable number of spins reported in Chapter II, but that sensitivity is possible only for optimum values of power and relaxation time, as explained in the appendix. The long relaxation time of ^{4}He requires the use of the spectrometer at very low powers, where it is relatively insensitive. An additional obstacle to observation of EPR of the metastable spins is their finite lifetime. No spectrometer, however sensitive at any power, can detect EPR of a spin system that is not relaxed within the lifetime of the spins. Electrons enter the 2^3S and $a^3\Sigma_u^+$ states with their spins equally likely to have $m_s = +1/2$ or $m_s = -1/2$. From this initially equal distribution, the populations of the spin states will tend to a Boltzmann distribution, approaching equilibrium with a time constant equal to the relaxation time. However, if the electrons leave the metastable states much before this time, the populations of the spin states will always be equal, and the EPR signal, proportional to the population difference, will be zero.

Hill, Heybey, and Walters measured metastable lifetimes of the order of a millisecond. The estimated relaxation time of pure ^{4}He is 10^3s, due to the dipole-dipole interaction between the metastable electrons and free electrons in the liquid. (See the appendix for this calculation.) Though the spin-dependent interactions in pure liquid ^{4}He are thus

much too weak to relax the metastable spin system, relaxation may be fast enough in a ^3He-^4He mixture. The relaxation time due to the hyperfine interaction between the ^3He nuclear spins and the metastable electron spins may be as low as .5 ms.

Even for a relaxation time of .5 ms, the problem of saturation remains. It is shown in the appendix that $T_1=T_2=.5ms$ implies saturation at a power of $6.5 \times 10^{-9}W$ in our spectrometer. That is, at powers higher than this, transitions stimulated by the microwaves appreciably lower the difference in populations of the $m_s = +1/2$ and $m_s = -1/2$ states and the signal is proportionately reduced. The best sensitivity to be achieved for this relaxation time is 10^{15} spins. Having taken into account the metastable lifetime, the relaxation time, and the dependence of sensitivity on power, we can now see that the maximum number of spins to be produced by electron bombardment in liquid ^3He-^4He is x300 smaller than the present spectrometer can detect.

This factor might be reduced by changing from a homodyne to a superheterodyne spectrometer. The r.f. bias and the r.f. power incident on the cavity would then be provided by two separate microwave generators 30MHz apart, so that the signal reflected from the cavity would beat with the bias. The output of the detectors would be a d.c. bias and a 30MHz signal

amplitude modulated at the frequency of the magnetic field. Since microwave diode noise decreases as 1/f for low frequencies, a superheterodyne system might have a noise figure 10dB smaller than the homodyne system. A further improvement in noise figure would result from a better system of klystron frequency stabilization. These two improvements might improve sensitivity by x10.

The remaining x30 increase in sensitivity necessary to detect a signal must be achieved by reducing the relaxation time by x30. This might be possible if liquid helium can be optically pumped. To use this relaxation technique, it would be necessary to illuminate the metastable helium atoms and molecules with circularly polarized resonance light travelling parallel to the static magnetic field. The light would pass through an axial hole in the magnet, Dewar windows 180° from the beam, and a hole in the cavity opposite the foil, be transmitted by the ground state liquid helium, and be absorbed by the excited states just in front of the foil. However, the absorption experiment of Hill, Heybey, and Walters indicated that the lifetimes of the metastable species would be so short as to preclude appreciable alteration of the spin state populations by optical pumping with available light sources, so this experiment has not yet been attempted.

Chapter IV

Hydrogen

In order to demonstrate proper performance of the apparatus in the null-result helium experiments discussed in the previous chapter, it was necessary to test the apparatus under approximately the same conditions but using a sample in which a signal could be detected. For this purpose, hydrogen was condensed and frozen in the closed microwave cavity at 4.2°K. A detectable number of hydrogen atoms were produced by a few seconds of elctron bombardment of the frozen molecules. Although the number of spins was not accurately known, this experiment did demonstrate that the apparatus could detect EPR in an irradiated substance at liquid helium temperatures.

A similar experiment had been reported by Piette, Rempel, Weaver, and Fluornoy[7] in 1959. They used a Varian V-4500 spectrometer and a 40MeV electron accelerator to detect EPR in hydrogen atoms frozen in solid H_2 at 4.2°K. Two 0.4Gauss lines 250 Gauss on either side of g = 2 were observed. The separation of these lines is due to the hyperfine interaction with the H nuclear spin. An optimum dose of 7.2×10^6 rad. on an 80mg sample produced 7.2×10^{16} spins. An increase in signal with increase in dose was recorded up to these optimum values, and further increase in dose reduced the number of

H atoms. They suggested that this decrease in signal was due to heating of the sample by the beam and poor thermal contact with the liquid helium bath. The irradiated region containing the H atoms was thermally isolated, and successive irradiations raised its temperature until the mobility of the atoms was sufficient to permit recombination and a decrease in the number of unpaired spins.

In the spectrum recorded with our apparatus, two 1.5 Gauss lines were spaced 510 Gauss apart. (See Figure 8, p. 38.) The maximum signal was produced by a dose of 6×10^5 rad on 6.3mg of frozen hydrogen. This optimum dose, smaller by x10 than in the experiment of Piette et al, might have been due to a higher rate of irradiation in our work or poorer thermal contact between the irradiated sample and the liquid helium bath. Assuming that one hydrogen atom is produced for every 500eV of irradiation, as reported by Piette et al, the sample we observed contained 4×10^{14} spins. The broadening of the lines was probably due to inhomogenities in the static magnetic field, perhaps caused by slight ferromagnetism of the Havar foil.

Successful in detecting EPR in solid hydrogen, we were led to consider liquid hydrogen as an appropriate substance with which to continue investigating the atomic properties of liquids. The interaction of atomic hydrogen with solid and liquid

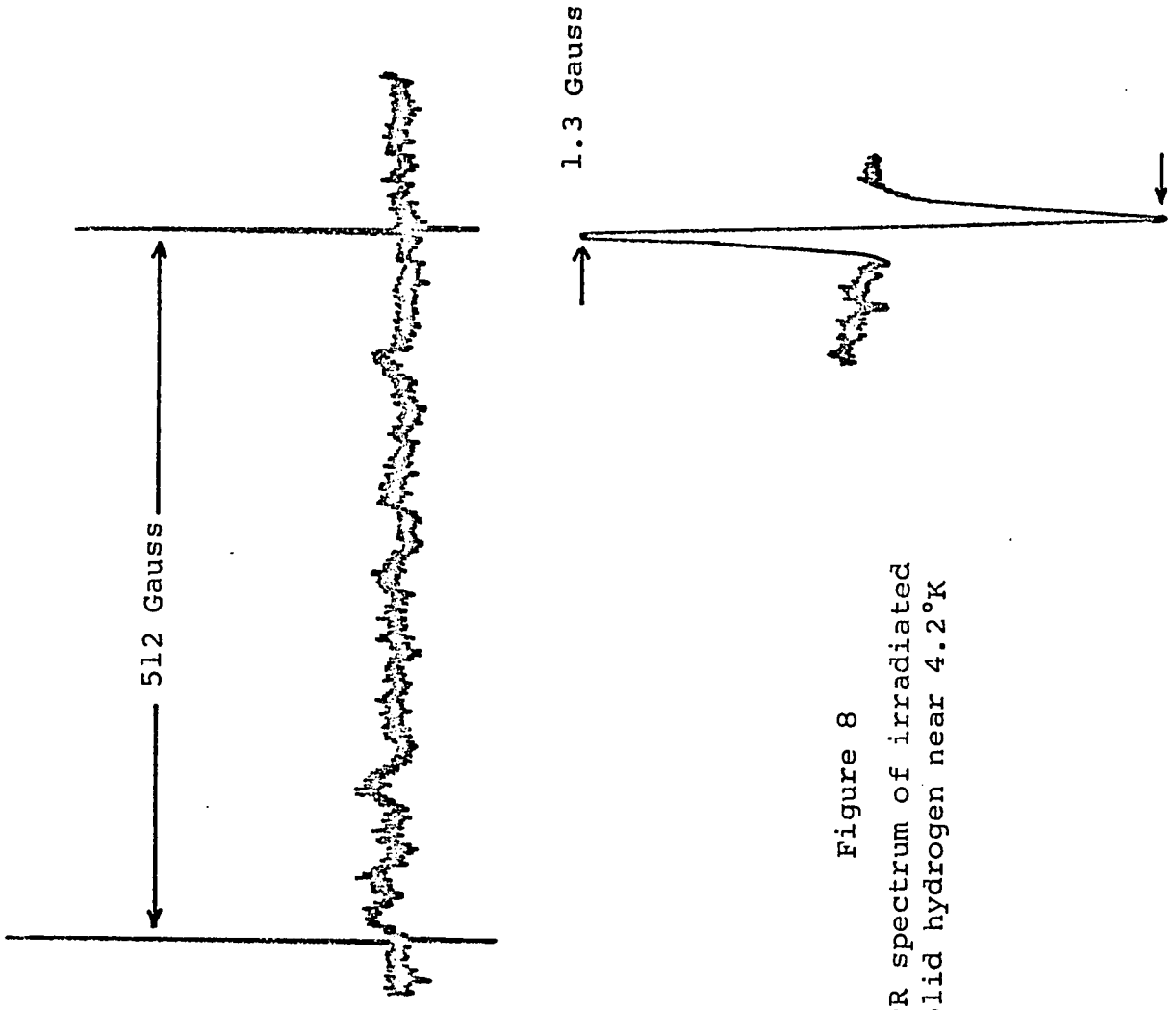

Figure 8

EPR spectrum of irradiated solid hydrogen near 4.2°K

environments might be studied by recording the EPR signal as a function of temperature. There were several instrumental difficulties involved in such experiments, however.

The temperature of a hydrogen bath could be varied from 12° K to 20° K by controlling the pressure above it. However, sublimation of a solid hydrogen sample cooled by a solid hydrogen bath caused the sample volume and cavity frequency to drift very rapidly.

Liquid hydrogen samples presented other problems. Boiling in liquid helium samples had been stopped by cooling them below 2.15° K, when the heat conductivity of helium became so huge that no thermal gradient existed sufficient to allow the formation of bubbles. Liquid hydrogen has no corresponding transition temperature or high heat conductivity, and therefore the sample will boil at equilibrium at all temperatures. Bubbles in the cavity caused random fluctuations in cavity impedance and reflected microwave power, and so were the cause of much noise. The only way to stop boiling was to cool the bath and sample far below 20.3° K (the boiling point at 1 atmosphere) by reducing the pressure above it for several minutes, and then quickly raise the pressure back to 1 atmosphere with warm gas. Until the liquid was warmed by heat leaks to 20.3° K, no boiling could occur.

This method for avoiding boiling noise created the

problem of temperature drift. Since the dielectric constant of hydrogen varies with temperature, the warming liquid caused a drift in cavity frequency and necessitated short experiments and frequent retuning of the spectrometer.

Even without these experimental difficulties, there were insufficient densities of atomic hydrogen created by electron bombardment of the liquid to permit observation of EPR with our instrument. This was demonstrated by the failure of several experiments and by the following theoretical analysis.

Assuming a yield of one hydrogen atom per 500eV, the production rate would be

$$\left.\frac{d[H]}{dt}\right|_{\text{production}} = I\,[H_2] \times 1.92 \times 10^{-9} \text{ moles/cc/sec.}$$

Where I is the beam current in nanoAmperes. A loss rate was reported by Bennett and Blackmore[16] for the reaction $2H+H_2 \rightarrow 2H_2$. Assuming that the reaction rate is proportional to the two-body collision rate, which is proportional to the mean particle velocity[17], their loss rate can be corrected for temperature.

$$\left.\frac{d[H]}{dt}\right|_{\text{loss}} = [H]^2\,[H_2] \times 4 \times 10^{15} \quad \frac{20.3^\circ K}{300^\circ K} \text{ moles/cc/sec .}$$

When the loss rate is equated to the production rate, the concentration of atomic hydrogen is found proportional to the square root of beam current. A beam of 1μA can be expected to produce only 10^{12} spins, fewer than our spectrometer can detect.

Thus, the absence of a signal in our experiment on liquid hydrogen was probably a consequence of rapid recombination of hydrogen atoms.

Chapter V

Biophysics

Hindered by instrument sensitivity and low sample density in attempts to extend our studies of the character of liquids, we considered the application of our apparatus to biophysical problems. Such a possibility was brought to our attention by the work of Robert J. Shalek of M. D. Anderson Hospital and Tumor Institute at Houston, Texas. He had used a pulsed electron accelerator and an optical absorption spectrometer to study the oxygen effect in electron-bombarded enzymes.[18] (The presence of oxygen in biological material usually increases their radiation sensitivity.) The equipment for his experiments was very similar to that we had used in our studies of the emission and absorption spectra of electron-bombarded liquid helium, and so our experience in liquid electronics was relevant to a set of problems in biophysics. Our more recently developed EPR apparatus might also be used in such studies, since some of the mechanisms present in irradiated biological samples involve formation of free radicals, which might exhibit EPR. As might be expected from the complexity of these samples, the effects of radiation on them are very involved. Figure 9, pp. 43 and 44 depicts part of the maze of physical, chemical, and biological effects that follow

	IONIZATION. EXCITATION.	RADICAL FORMATION. BOND RUPTURES.	RADICAL REACTIONS. CHANGES IN GEOMETRY.
		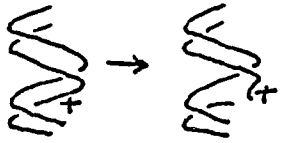 Single strand break in DNA	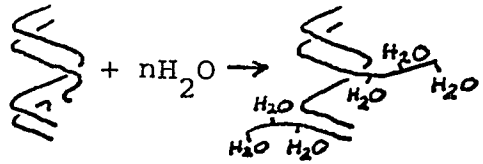 Water unzips hydrogen bonds
Direct action	$e^- + M \rightarrow 2e^- + M^+$ Primary & secondary ionization	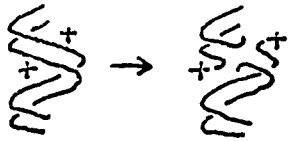 Double strand break in DNA	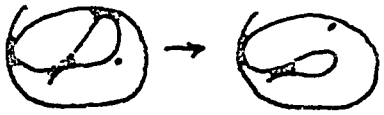 Intramolecular radical migration in an enzyme
		$M_1 - M_2^+ \rightarrow M_1^{\cdot} + M_2^+$ Fragments break off	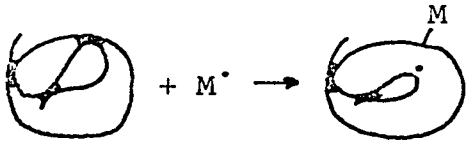 Intermolecular radical transfer to an enzyme
Indirect action	$e^- + H_2O \rightarrow 2e^- + H_2O^+$ Primary & secondary ionization	$H_2O^+ \rightarrow H^+ + OH^{\cdot}$	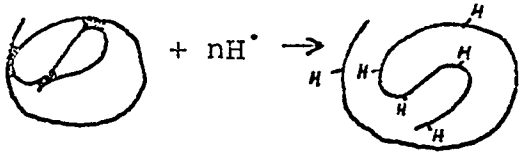 Reduction of disulfide bonds in an enzyme
	$e^- + H_2O \rightarrow e^- + H_2O^*$ Secondary excitation	$H_2O^* \rightarrow H^{\cdot} + OH^{\cdot}$ Dissociation	$MH + H^{\cdot} \rightarrow MH_2$ $\rightarrow M^{\cdot}{}_2 + H_2$ $MH + OH^{\cdot} \rightarrow MHOH^{\cdot}$ $\rightarrow M^{\cdot} + H_2O$

Figure 9

Typical mechanisms present in irradiated biological systems

REPAIR OF RADIATION DAMAGE.
OXYGEN EFFECT.

EFFECTS OF DAMAGE ON
REPLICATION, ENZYME ACTION,
& PROTEIN SYSTHESIS.

METABOLIC EFFECTS.
GENETIC EFFECTS.

$MH^+ + e^- \rightarrow MH$

Repair by hydrated electron

$M^\cdot + HSR \rightarrow MH + {}^\cdot SR$

Repair by sulfhydryl group

$M^\cdot + H^\cdot \rightarrow MH$

Repair by hydrogen

$e^- + .O_2 \rightarrow O_2^-$

$H^\cdot + O_2 \rightarrow HO_2^\cdot$

Scavenging of agent
of repair by oxygen

$M^\cdot + O_2 \rightarrow MO_2^\cdot$

Peroxidation &
confirmation of damage

Figure 9 (continued)

Typical mechanisms present in irradiated biological systems

irradiation of organic macromolecules. A first degree of order is brought to this group of effects by considering them roughly in the order in which they occur.[19] It will be seen that the earliest links in the chain of events are those most susceptible to investigation with the techniques of physics.

The first effect of electron-bombardment is likely to be ionization, either of an electron on a biological molecule (enzyme, protein, nucleic acid, amino acid, etc.) or of an electron on a solvent molecule (H_2O). In the first case the irradiation affects the macromolecule by direct action. The second case is the first step of indirect action if the solvent ion enters a chain of reactions which involve macromolecules. The electrons released by ionization may also affect the macromolecules by indirect action. Slow secondary electrons may induce polarization of nearby water molecules, which isolates and further slows the electrons, leading to 'hydrated electrons'. These are fairly stable, can diffuse long distances, and can enter into chemical reactions with positive ions or electronegative atoms.

In the second group of reactions, radicals are formed by dissociation of ionized and excited molecules. Macromolecules may be broken into fragments, or bonds may be broken to change internal structure. For example, the phosphate bond between two sugars in a strand of DNA may be ruptured,

separating that strand into two fragments which are held to the other, unbroken strand by hydrogen bonds.

In the third group, structural changes follow from reactions in which water molecules break hydrogen bonds and hydrogen radicals reduce the disulphide bonds which hold proteins in their characteristic folded configurations. Other macromolecules may be damaged by solvent radicals (indirect action), and the damage sites can migrate to sulphur atoms elsewhere on the molecule.

Radiation damage may be repaired by reactions of the fourth group involving hydrated electrons, sulphhydryl groups, and hydrogen. These mechanisms may be hindered by oxygen, which competes with the macromolecules for the electrons and hydrogen, and which may peroxydize a macromolecule before it is repaired in a reaction with hydrogen orsulphhydryl.

Many of the reactions mentioned here may be studied by EPR, since they involve radicals which live long enough to undergo magnetic relaxation. The oxygen effect in lysozyme was chosen as the first biophysical reaction which our apparatus would be used to investigate. This effect is of interest because elucidation of its mechanisms may shed light on the larger processes of radiation damage and repair. In turn, information about radiative inactivation may answer questions about the mechanisms of undamaged enzymes, nucleic acids, and

other biological structures. As well as being relevant to basic investigations of general biological processes, the oxygen effect may be of practical use in radiation therapy of cancer. It has been suggested that anoxic (oxygen-starved) centers of tumors may be resistant to radiation and thus able to regenerate the tumor after therapy. Knowledge of the manner in which oxygen sensitizes molecules to radiation may lead to more effective treatment of cancer. The enzyme lysozyme was chosen as the substance in which to study the oxygen effect, because it has been comparatively well studied and information about its action and structure may aid our investigations.

The preliminary step in this work was modification of the microwave cavity to accept dry lysozyme or lysozyme solutions. The losses associated with the motion of electric dipoles in a microwave electric field had not been a factor in the hydrogen and helium experiments, since these substances have no permanent electric dipole moments. Cavity Q was greatly reduced by as much as 1 cm^3 of dry lysozyme or .01 cm^3 of water, however. Dielectric losses could be minimized by using small samples close to the cavity wall, where the r.f. electric field is close to zero. A further improvement in Q was obtained by increasing the cavity volume. A full wave cavity was constructed, as shown in Figure 10, p. 48, with a removable iris, to permit matching the cavity to the

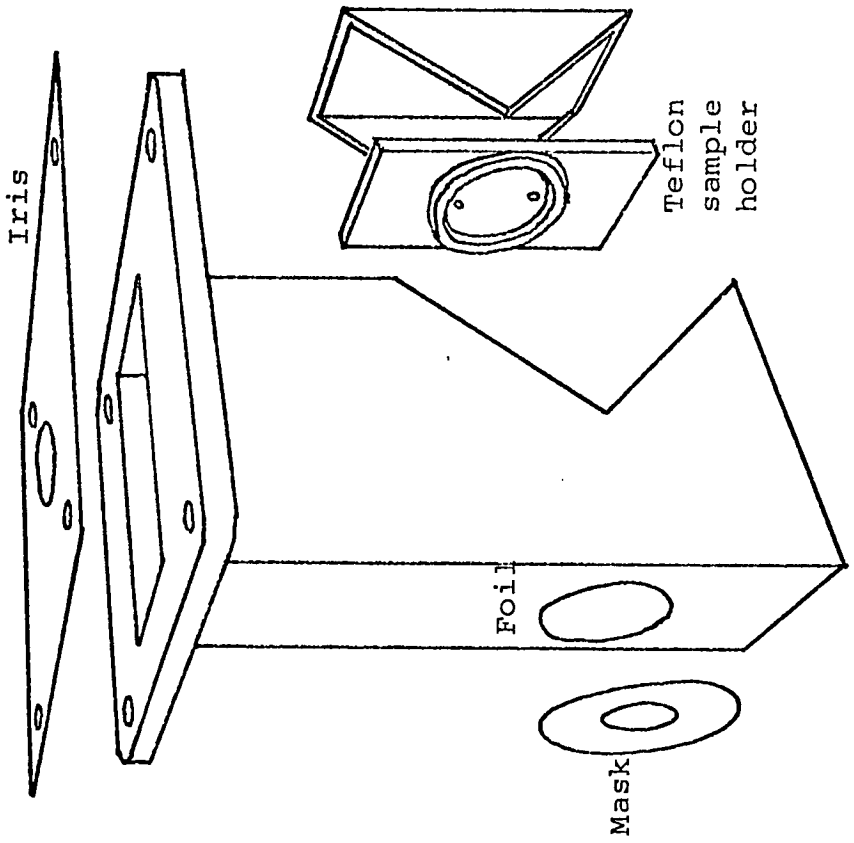

Figure 10

Microwave cavity & sample holder for detection of EPR in irradiated lysozyme solutions

spectrometer for different samples. To hold liquid samples, the small piece of Teflon shown in Figure 10 was pressed against the front wall of the cavity, forming a thin cylindrical volume between the foil and the Teflon. A solution of lysozyme was injected through the lower hole until it began to spill out through the top hole. Surface tension kept this .03 cm^3 drop from draining out through the lower hole. The thickness of this drop, about .3 cm, was sufficient to stop the electron beam before it could reach the back of the sample holder. A mask of 3/16"ID in front of the foil shielded the sides of the Teflon sample holder from the beam, preventing the formation of defects in the Teflon which would give a spurious EPR signal. A deeper sample holder was used for dry losozyme samples, since the range of the beam in a powder was likely to be longer than in water.

An EPR signal was detected in solid lysozyme after irradiation of about 6×10^6 rad. (The sample weight was estimated at .01g by weighing the lysozyme powder which had turned brown, a volume of approximately .05 cc.) The signal did not increase much after 2×10^7 rad, when there were about 10^{14} spins in the sample. There was a single line 16 Gauss wide at g = 2. A line of this width and g-value was also seen by Shalek in 1961 in lysozyme irradiated with X-rays at 77°K and aged at 300°K.[20]

Dry lysozyme was used as a sample more to test the system than to study radiation damage. It is difficult to control the exposure of dry samples to atmospheric oxygen in our apparatus, and the mobility of reactants in a powder is unknown and probably irregular. Also, a dry sample does not resemble the situation of macromolecules in living cells. As discussed in Chapter II, with a powdered sample in the cavity, the foil could jitter at the modulation frequency, causing a lot of noise. All these factors make lysozyme solutions much more useful samples than dry lysozyme.

A saturated water solution of lysozyme (about 10^{-4} molar for a molecular weight of 15,000) irradiated by various beam currents yielded no detectable EPR signal. The earlier work of Shalek led us to suspect that oxygen dissolved in our lysozyme solution might have reduced the EPR signal below the sensitivity of our spectrometer. Davies, Ebert, and Shalek[18] found two broad absorption features near 3100 Å and 4000 Å in lysozyme solutions subjected to pulse radiolysis. These features were greatly attenuated by adding small amounts of oxygen to the solution before irradiation. The intermediate species responsible for this optical absorption had lifetimes of the order of milliseconds and might have been radicals, with an EPR spectrum.

In our next experiment, therefore, the lysozyme

solution was de-oxygenated by bubbling argon through it for an hour, and it was judged unlikely that atmospheric oxygen could appreciably diffuse into the sample. A second attempt to detect EPR in continuously irradiated lysozyme solution was also unsuccessful.

It was not feasible to increase the number of spins in the sample by increasing the dose rate, since even moderate beam currents boiled the tiny sample. At 147keV, a beam current of 1μA deposits 3.5×10^{-2} calories/s into .03 cm^3, or 1.2 calories/cm^3/s. A thermally insulated sample would thus boil in 1 minute. Experimentally it was determined that water was forced out of the holes in the sample holder (altering the cavity Q and frequency) after 5 min of a .15μA beam or 10 min of a .03μA beam.

In order to increase the number of spins without overheating the sample, pulsed high beam currents and a signal averaging device are planned for future experiments. A modified sample holder will be used, to permit quick replacement of the radiation-damaged and -heated sample with fresh solution between pulses. After sufficient pulses to average out noise, the static magnetic field will be increased a step. A series of such measurements will give a set of points of reflected microwave power v.s. magnetic field (i.e., the EPR spectrum). By varying the delay after a pulse when the

signal averager is turned on, the time variation in EPR may be obtained. This will hopefully provide information about the location of unpaired spins and the paths they follow in the reactions following irradiation of enzyme solutions.

Appendix A

Spectrometer Sensitivity

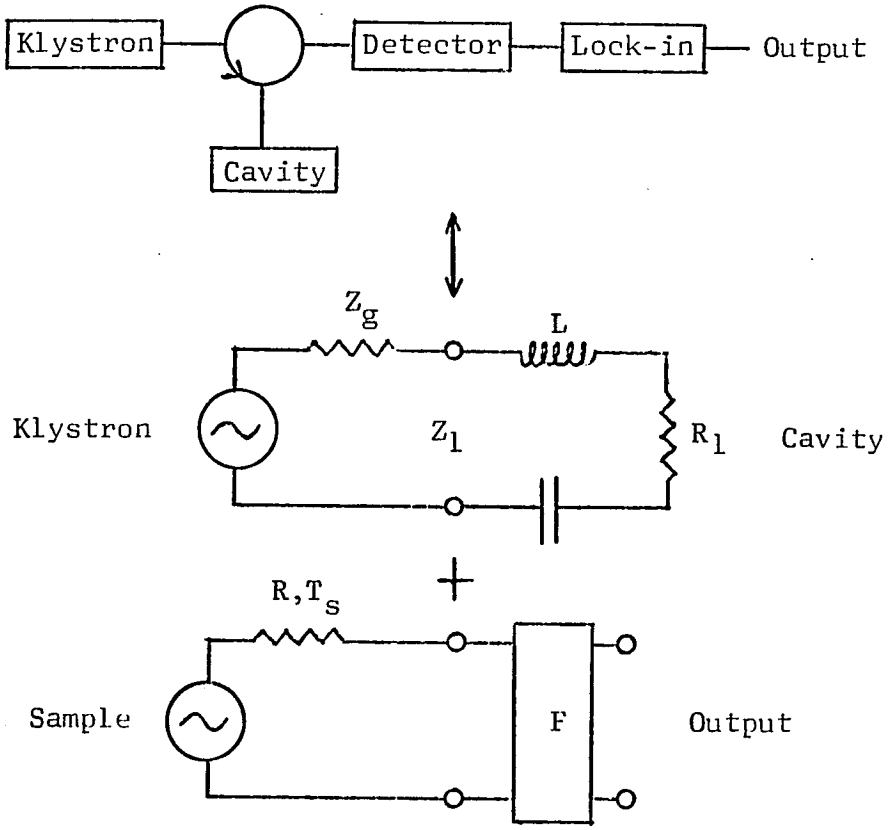

Figure 11

Equivalent circuits of reflection spectrometer

The object of this appendix is to relate the output signal of the spectrometer to the sample characteristics. We shall assume that the waveguide and cavity are analogous to a transmission line and an LRC circuit and use the simple techniques of a.c. circuit analysis to calculate the signal.[21,22]

Since there is no analog of a microwave circulator, we need one a.c. circuit as a model for the system between the klystron and the sample and another a.c. circuit to represent the system from the sample to the lock-in amplifier output. (See Figure 11.) In the latter circuit, a signal at the modulation frequency is generated at the sample, passes through a device of noise figure F, and is recorded. The noise figure is defined as the ratio of input and output signal-to-noise ratios.

$$F = \frac{S/N|in}{S/N|out}$$

The smallest detectable sample will give $S/N|out = 1$, so this sample will give a signal power at the sample of $S_i = FN_i$. If the sample is equivalent to a generator of resistance R and the temperature T_S, the open circuit noise power it emits is $4kT_S\Delta f$. When matched with a load R the power transferred to the load is $kT_S\Delta f$. The smallest detectable sample will therefore generate a signal power $S_i = FkT_S\Delta f$.

The first equivalent circuit will be used to calculate this signal from the magnetic properties of the sample. In this circuit, the voltage reflected from the load is

$$E_r = E\,\frac{Z_g - Z_1}{Z_g + Z_1}$$

where the voltage incident on the load is E, and Z_g and Z_1 are the waveguide and load impedances. If the load is resonant

and matched to the generator, $Z_g = Z_l = R$, and $E_r = E \frac{\Delta R}{2R}$, where ΔR is the change in load resistance due to EPR absorption of the sample. The quality factor of the load is $Q = \frac{\omega_0 L}{R}$, so EPR changes this by $\Delta Q = -Q \frac{\Delta R}{R}$, and we see that $E_r = -E \frac{\Delta Q}{2Q}$.

To calculate Q, we return to the definition of quality factor for a cavity,

$$Q = \frac{\omega_0 \times \text{stored energy}}{\text{average power lost in cavity walls, through iris, and in sample}}$$

We see that

$$\frac{1}{Q} = \frac{1}{Q_u} + \frac{1}{Q_\chi},$$

where Q_u is the unloaded Q, or cavity Q with no EPR, and Q_χ is due to power lost in the sample. The r.f. energy absorbed by the sample when its susceptibility increases is equal to the work done to increase the magnetization in the presence of a magnetic field,

$$dW = \bar{H} \cdot d\bar{B}\, dv.$$

The average power lost in the sample is thus

$$\frac{1}{2\pi} \int_0^{2\pi} d\omega t \int_{\text{sample}} \bar{H} \cdot \frac{d\bar{B}}{dt}\, dv.$$

The magnetic field is the sum of the large static field H_0 and the small microwave field $2H_1$,

$$\bar{H} = H_0\hat{z} + 2H_1\hat{x}\cos\omega t.$$

The magnetization includes a static component $\chi_0 H_0\hat{z}$ and an r.f. component, which lags the applied field, so that there is an in-phase component $2\chi' H_1\hat{x}\cos\omega t$ and an out-of-phase component $2\chi'' H_1\hat{x}\sin\omega t$.

$$\bar{B}=\mu_0(\bar{H}+\bar{M}) =\mu_0(H_0\hat{z}+2H_1\hat{x}\cos\omega t+\chi_0 H_0\hat{z}+2\chi' H_1\hat{x}\cos\omega t+2\chi'' H_1\hat{x}\sin\omega t)$$

$$\frac{1}{2\pi}\int_0^{2\pi} d\omega t\ \bar{H}\cdot\frac{d\bar{B}}{dt} = \frac{1}{2\pi}\int_0^{2\pi} d\omega t\,\mu_0\omega 4H_1^2(-\sin\omega t\cos\omega t-\chi'\sin\omega t\cos\omega t+\chi''\cos^2\omega t)$$

$$= 2\mu_0\omega\chi'' H_1^2$$

Therefore, the sample Q is

$$Q_\chi = \frac{\omega_0\ 2\mu_0\int_{\text{cavity}} H_1^2 dv}{2\omega_0\mu_0\chi''\int_{\text{sample}} H_1^2 dv} = \frac{1}{\chi''\eta},$$

where η is the filling factor. We thus find that the change in Q due to the sample susceptibility is

$$-\frac{1}{Q^2}\Delta Q = \frac{1}{Q_\chi} = \chi''\eta\ .$$

This gives the reflected voltage in terms of sample and cavity properties,

$$E_r = \frac{1}{2}E\chi''\eta Q_u.$$

The reflected power is $\left(\frac{E_r}{Z_1}\right)^2 R = \left(\frac{E_r}{R}\right)^2 R_g$ and the incident power is $P_w = \left(\frac{E}{Z_1}\right)^2 R_1 = \frac{E^2}{R}$. The signal power is thus $S_i = \frac{1}{4}P_w(\chi''\eta Q_u)^2$,

and for an output signal-to-noise ratio of 1,

$$\frac{1}{4}P_w\ (\chi''\eta Q_u)^2 = FkT_s\Delta f.$$

The r.f. susceptibility may be calculated from Bloch's equations[23], and has a maximum value at ω_o of

$$\chi''_{max} = \frac{1}{\sqrt{3}}\chi_o \frac{B_o}{\Delta B_{pp}},$$

where B_o is the static magnetic induction field at EPR and ΔB_{pp} is the peak-to-peak width of the first derivative of the absorption line. The static susceptibility χ_o of N_{min} spins of volume V_s and temperature T_e may be calculated using Maxwell-Boltzmann statistics.[23]

$$\chi_o = \frac{N_{min}}{V_s}\frac{\mu_o g^2\beta^2}{4kT_e}$$

The minimum detectable sample thus contains

$$N_{min} = \frac{8kT_e V_s}{\eta Q_u \mu_o g^2\beta^2}\ \frac{\Delta B_{pp}}{B_o}\ \sqrt{\frac{3FkT_s\Delta f}{P_w}}\quad \text{spins.}$$

The conditions under which the spectrometer sensitivity were measured give the following parameters:

$k = 1.38 \times 10^{-23}$ Joules/°K

T_e = electron spin temperature = 300°K

η = filling factor = $1/2\ \frac{V_s}{V_c}$

V_c = cavity volume = $5.3 \times 10^{-6} m^3$

$Q_u = 2000\ \pm 10\%$

$\mu_o = 4\pi \times 10^{-7}$

$g = 2$

$\beta = 9.28 \times 10^{-24}$ Joule $-m^2$/Weber

$\Delta B_{pp} = 1G$

$B_o = 3000G$

F = noise figure = 100 $\pm 50\%$

T_s = sample noise temperature $\doteq 300^\circ$ K

Δf = lock-in bandwidth = .1Hz at RC = 1 second $\pm 25\%$

P_w = incident power = 10^{-3}W

$N_{min} = 1.5 \times 10^{12}$ spins $\pm 20\%$

Appendix B

Field Modulation

In the preceding calculation it was assumed that a signal with amplitude equal to the difference between on-resonance and off-resonance reflected microwaves was amplified by a device of bandwidth $\Delta f \sim 0.1$Hz. In practice, microwaves are not amplified, but are rectified by diodes; and instead of trying to amplify the d.c. signal from the diodes with a bandwidth of only 0.1Hz, the reflected signal is modulated at an intermediate frequency and an i.f. amplifier is used. In this section, we shall relate signal amplitude to modulation field amplitude.

The reflected voltage is related to the static magnetic field by a line shape function g(B).

$$Er = 1/2\ E\eta Q_u \chi'' = 1/8\ E\eta Q_u \chi_o \omega_o Z g(B) \equiv Ag(B).$$

The magnetic field B is the sum of a slowly increasing field B_o and a modulation field $B_m \cos\omega t$. After expanding g(B) about B_o in a Taylor's series, the reflected voltage is

$$Er = A\left[g(B_o) + g^{(1)}(B_o) B_m \cos\omega t + \frac{1}{2!} g^{(2)}(B_o) B_m^2 \cos^2\omega t + \ldots\right].$$

The powers of $\cos\omega t$ can be written as sums of cosines of integral multiples of ωt, and so we may regroup this series to get

$$Er = A\left[g(B_o) + \cos\omega t\left(g^{(1)}(B_o) B_m + \frac{1}{8} g^{(3)}(B_o) B_m^3 + \frac{1}{192} g^{(5)}(B_o) B_m^5\right) + \cos 2\omega \ldots\right]$$

Since the lock-in will amplify only the signal at angular frequency ω, the only relevant reflected voltage has the amplitude

$$E_r = A\left[g^{(1)}(B_o)B_m + \frac{1}{8}g^{(3)}(B_o)B_m^3 + \frac{1}{192}g^{(5)}(B_o)B_m^5 + \ldots\right].$$

By solving Bloch's equations[23] the function $g(B_o)$ is found to be

$$g = \frac{2T_2}{1 + (\gamma B_o - \omega)^2 T_2^2}.$$

If we define the line width $\Delta\omega_{pp}$ as the peak-to-peak width of the first derivative of g, and set $\Delta B_{pp} \equiv \frac{\Delta\omega_{pp}}{\gamma}$, $B \equiv \frac{B_m}{\Delta B_{pp}}$, and $W \equiv \frac{\omega_o - \omega}{\Delta\omega_{pp}}$, then $T_2 = \frac{2}{\sqrt{3}\,\Delta\omega_{pp}}$ and

$$E_r = A\left[\frac{-\frac{16}{3}T_2WB}{\left[1+\frac{4}{3}W^2\right]^2} - \frac{\frac{32}{3}T_2WB^3\left[\frac{4}{3}W^2 - 1\right]}{\left[1 + \frac{4}{3}W^2\right]^4} - \frac{\frac{160}{9}T_2WB^5\left[\frac{16}{9}W^4 - \frac{4}{9}W^2 + 1\right]}{\left[1 + \frac{4}{3}W^2\right]^6} - \ldots\right].$$

The maximum value of this expression is to be compared to the result of the earlier analysis,

$$E_r = Ag(B)_{max} = A2T_2.$$

Since $N_{min} \propto \chi_o \propto E_r$, the ratio of the two values of E_r is the factor by which the first estimate of N_{min} is too big.

For vanishingly small modulation fields, $B \ll 1$ and

$$E_r = A\left[\frac{-\frac{16}{3}T_2WB}{\left[1 + \frac{4}{3}W^2\right]^2}\right].$$

This is maximized for $W = \pm 1/2$ $\left(\omega = \omega_o \pm \frac{\Delta\omega_{pp}}{2}\right)$, when

$$E_r = \pm \frac{3}{2} T_2 BA.$$

The correction factor is then $C = \frac{3}{4} B = \frac{3}{4} \frac{B_m}{\Delta B_{pp}}$.

The experimentally observed relations of line height and line width to modulation field are described by Figure 12.

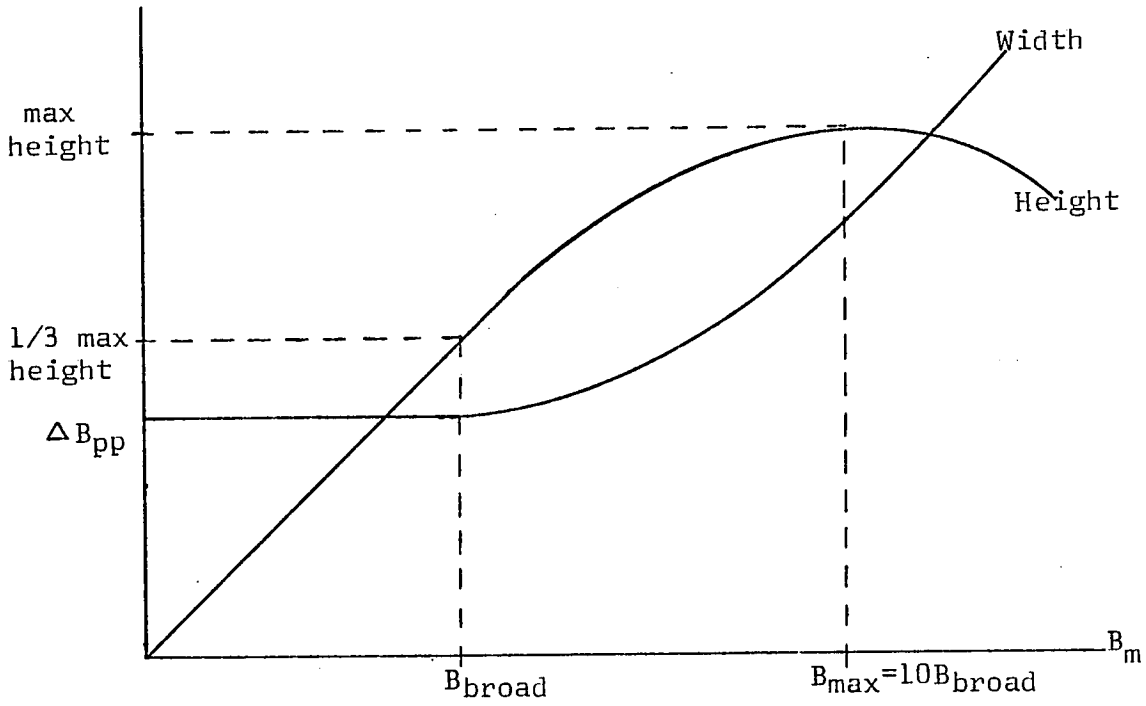

Figure 12

EPR signal v.s. modulation field

It would be desireable to calculate the value of the modulation field B_{max} which maximizes the the line height and to evaluate the correction factor for this optimum value of B. This would give a theoretical value for the minimum number

of observable spins using field modulation. However, such a calculation is impractical, since for $B = \frac{B_{max}}{\Delta B_{pp}}$ the B^3 and B^5 terms in the expansion of E_r are of the same order as the B term. To be accurate, therefore, the series would have to be expanded much further.

A less rigorous relation may be deduced from two experimental observations. The modulation field B_{broad} at the onset of line broadening is about one tenth the true line width ΔB_{pp}, and increase of the modulation field from B_{broad} to B_{max} can increase the line height by about a factor of three. Since $B = \frac{B_{broad}}{\Delta B_{pp}} \sim \frac{1}{10} \pm 20\%$, we can ignore the B^3 and B^5 terms and use the correction factor $C = \frac{3}{4}\frac{B_m}{\Delta B_{pp}} = \frac{3}{40}$. Since the line height can be increased by $\times 3 \pm 20\%$, the optimum correction factor is about $C = \frac{9}{40} \pm 30\%$. The minimum detectable number of spins using field modulation is then $\frac{40}{9} N_{min} = 6.7 \times 10^{12}$ spins $\pm$ 35%. This agrees with the experimental result discussed on p. 28, $1/3 \times 1.5 \times 10^{13} = 5 \times 10^{12}$ spins.

Appendix C

Saturation

The effect of saturation may reduce the sensitivity of the spectrometer below the values calculated in Appendix A and Appendix B. It has been assumed so far that the maximum value of the r.f. susceptibility is

$$\chi''_{max} = \frac{1}{\sqrt{3}} \chi_o \frac{B_o}{\Delta B_{pp}} ,$$

a relation which is correct only for r.f. powers below saturation. In this section we shall examine the relation between sensitivity and power.

By solving Bloch's equations in the slow passage case, we find that the r.f. susceptibility is

$$\chi'' = \frac{1/2 \quad \chi_o \omega_o T_2}{1 + (\omega-\omega_o)^2 T_2^2 + \gamma^2 B_1^2 T_1 T_2} .$$

(For low power, $\gamma^2 B_1^2 T_1 T_2 \ll 1$, and χ'' reduces to the form used in deriving our previous results.) It may be shown that if all power incident on the cavity is absorbed in the walls, the power is related to the peak r.f. field by $P_w = aB_1^2$, where 'a' is a constant. For our cavity, $a = 5.0 \times 10^7 \text{Watts/Tesla}^2 = .5 \text{ Watts/Gauss}^2$.

The voltage reflected from the cavity is then

$$E_r = \frac{1}{2} E \eta Q_u \chi'' \propto \frac{\sqrt{P}}{1 + bPT_1T_2} \quad \text{for a constant b,}$$

and the minimum detectable sample is

$$N_{min} \quad \frac{1 + bPT_1T_2}{\sqrt{P}} \cdot$$

According to this relation, the minimum number of spins will decrease as power is increased, until $bPT_1T_2 \sim 1$. For higher powers, the minimum number of spins will increase. Thus the sensitivity is limited by long relaxation times.

Sensitivity does not increase without limit as T_1 and T_2 are decreased, however, since the noise figure is also power dependent. For high powers, klystron FM noise demodulated by the cavity is the principal noise source, and $F \propto P$ for $P > 0.1$ mW in our spectrometer. Thus,

$$N_{min} \propto \frac{1 + CPT_1T_2}{\sqrt{P}} \quad P < 0.1\text{mW}$$

and $$\propto 1 + CPT_1T_2 \quad P > 0.1\text{mW}.$$ Even for the shortest relaxation times, no increase in sensitivity is possible above 0.1mW. The dependence of sensitivity on power is sketched in Figure 13.

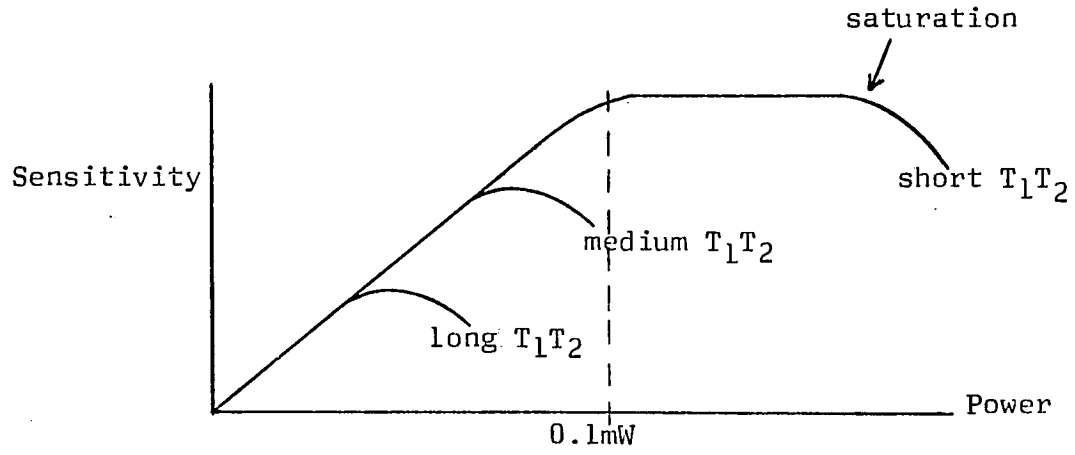

Figure 13

Sensitivity v.s. Power

Appendix D

Relaxation

We have calculated the sensitivity of our spectrometer using straight detection for samples which do not saturate at 1mW, have corrected this calculation for field modulation, and have derived the qualitative behavior of sensitivity with power. We shall now make a quantitative estimate of the relaxation times and calculate the spectrometer sensitivity for the optimum power and modulation field.

The longitudinal relaxation time T_1 is the time constant of the approach to equilibrium of the z-component of magnetization.

$$\frac{dMz}{dt} = \frac{Mo - Mz}{T_1}$$

In the analysis of Bloembergen, Purcell, and Pound[23] T_1 is related to W, the average probability per unit of time of a transition between spin states, by

$$T_1 = \frac{1}{2W} .$$

If the initial spin state is $|\sigma(o)\rangle = |+\rangle$, then

$$W = \frac{d}{dt} |\langle - |\sigma(t)\rangle|^2 .$$

We expand $|\sigma(t)\rangle$ in terms of the eigenfunctions of the

Zeeman Hamiltonian $\mathcal{H}_0$,

$$|\sigma(t)\rangle = C_-(t)\, e^{-i\omega_- t} \,|->\, + C_+(t)\, e^{-i\omega_+ t} \,|+\rangle$$

From Schrodinger's equation

$$i\hbar \frac{d}{dt} |\sigma(t)\rangle = (\mathcal{H}_0 + \mathcal{H}_1(t)) \,|\sigma(t)\rangle$$

we derive

$$i\hbar \frac{d}{dt} C_-(t) = C_-(t) \langle -|\mathcal{H}_1(t)|-\rangle + e^{-i(\omega_+ - \omega_-)t} C_+(t) \langle -|\mathcal{H}_1(t)|+\rangle .$$

In the first approximation, the coefficients $C_\pm(t)$ on the right are given their values at $t = 0$ and the equation is integrated.

$$\frac{dC_-(t)}{dt} = \frac{1}{i\hbar} e^{-i\omega t} \langle -|\mathcal{H}_1|+\rangle$$

$$C_-(t) = \frac{1}{i\hbar} \int_0^t \langle -|\mathcal{H}_1(t')|+\rangle \; e^{-i\omega t'} dt'$$

For times close to $t = 0$, the transition probability per unit time is thus

$$W = C_-(t) \frac{dC_-^*(t)}{dt} + \text{c.c.}$$

$$= \frac{1}{\hbar^2} \int_0^t \langle +|\mathcal{H}_1(t)|-\rangle \langle -|\mathcal{H}_1(t')|+\rangle \, e^{-i\omega(t'-t)} dt' + \text{c.c.}$$

The only terms of the Hamiltonian that will contribute to W are those containing σ_x and σ_y.

In many substances, such a term is provided by the interaction of the electron spin with the nuclear spin of a neighboring atom. In ^{4}He there is no nuclear spin, however,

and the only relaxing interactions are those of the metastable electron spin with free electrons and with other metastable spins. It will be shown that these interactions do not relax the metastable spin system, because the lifetime of a metastable state is less than the relaxation time.

The population N_+ of the $m_s = +1/2$ spin state of a collection of helium metastable molecules is affected by four processes. Relaxation mechanisms lead to

$$\left.\frac{dN_+}{dt}\right|_1 = N_-W_- - N_+W_+ \quad ,$$

where the transition probabilities W_+ and W_- are related by a Boltzmann factor,

$$W_-/W_+ = e^{-\frac{\hbar\omega}{kT}} \quad .$$

Transitions stimulated by microwaves at the Larmor frequency account for

$$\left.\frac{dN_+}{dt}\right|_2 = (N_1 - N_+)\ P \ ,$$

where the probability per second P of a stimulated transition is

$$P = \frac{1}{4}\gamma^2 B_1^2 g(\omega) \ .$$

The destruction of metastable states with lifetime τ is the third process, giving

$$\left.\frac{dN_+}{dt}\right|_3 = -\frac{N_+}{\tau} \ .$$

Metastable molecules are created X per second, half with m_s=+1/2

and half with $m_s = -1/2$, so that

$$\left.\frac{dN_+}{dt}\right|_4 = \frac{1}{2} X.$$

The total rate of change of $m_s = +1/2$ spins is thus

$$\frac{dN_+}{dt} = N_-W_- - N_+W_+ + (N_- - N_+)P - \frac{N_+}{\tau} + \frac{1}{2} X.$$

When the corresponding equation for the $m_s = -1/2$ spins is subtracted from this, we have

$$\frac{d(N_+ - N_-)}{dt} = 2N_-W_- - 2N_+W_+ - 2(N_+ - N_-)P - \frac{(N_+ - N_-)}{\tau} .$$

Since $\hbar = 6 \times 10^{-17}$ ergs, while $k \times 1.5^\circ K = 2 \times 10^{-16}$ ergs, the Boltzmann factor is approximately

$$e^{-\frac{\hbar\omega}{kT}} \sim 1 - \frac{\hbar\omega}{kT} ,$$

and for the change in the excess population $n = N_+ - N_-$ we get

$$\frac{dn}{dt} = \frac{n_o - n}{T_1} - n\frac{1}{2}\gamma^2 B_1^2 g(\omega) - \frac{n}{\tau} \quad , \quad \text{where}$$

$n_o = \frac{(N_+ + N_-)\hbar\omega}{2kT}$. The steady state excess population is

$n_s = n_o(1 + \frac{1}{2}\gamma^2 B_1^2 T_1 g(\omega) + \frac{T_1}{\tau})^{-1}$. Thus the finite lifetime of the metastable spins shows up in the saturation factor, and our earlier relation for the minimum number of spins must be modified to give

$$N_{min} \propto \frac{1 + bPT_1T_2 + \frac{T_1}{\tau}}{\sqrt{P}} .$$

Unless $T_1 \ll \tau$, the system will be saturated at all powers.

The lifetime of the $a^3\Sigma_u^+$ metastable helium molecule was measured by Hill, Heybey, and Walters.[6] They found that a beam current of 1μA led to a steady state concentration of 10^{13} metastable molecules per cm^3 in a volume of .05 cm^3. The lifetime of this species was limited by metastable-metastable collisions, and for the above conditions, the lifetime was 7×10^{-4}s. The spin system will always be saturated, therefore, unless $T_1 \ll 7 \times 10^{-4}$s.

We shall consider several interactions $\mathcal{H}_1(t)$ which tend to relax the metastable spin system. The weakest interaction to be calculated is that of the metastable spin with the beam current. A stronger interaction is that between the metastable spins and the spins of the secondary electrons. The strongest interaction in pure liquid ^{4}He is between the metastable spins, but since metastable states are destroyed by such encounters, they cannot be effective in relaxing the spin system. (Using the kinetic theory of gases, the time between metastable-metastable collisions may be calculated to be 3×10^{-4}s. Since the metastable lifetime is 7×10^{-4}s, each spin will on the average have only one interaction tending to relax it before it is destroyed in the next encounter.

The metastable-metastable relaxation mechanism competes with itself.)

The interaction of a spin with the current of a beam electron is

$$\mathcal{H}_1(t) = -\bar{\sigma} \cdot \bar{B}$$

where

$$\bar{B} = \frac{\mu_0 ev \sin\theta(t)}{4\pi r(t)^2} \hat{x}$$

is the magnetic field at the origin due to a spinless electron moving with velocity $v\hat{z}$ at a point r,θ.[24] For times very close to t = 0, the probability per second of a transition during the passage of one beam electron is

$$w = \frac{2t}{\hbar^2} \quad | \langle + | \mathcal{H}_1(t) | - \rangle |^2 .$$

The time t during which $\mathcal{H}_1$ is effective is approximately r/v, where r is the distance of closest approach. The probability of a transition in this encounter is thus

$$tw \simeq \frac{2}{\hbar^2}\left(\frac{r}{v}\right)^2 \left(\frac{\beta\mu_0 ev}{4\pi r^2}\right)^2 = \frac{4 \times 10^{-30}}{r^2} .$$

The total probability of a transition due to all encounters occuring in one second is

$$W = 4 \times 10^{-30} \sum_{i=1}^{N} \frac{1}{r_i^2} .$$

To calculate the average

$$\overline{1/r^2} = \int_0^\infty \frac{1}{r^2} \rho\left(\frac{1}{r^2}\right) d\frac{1}{r^2} ,$$

we need the distribution function $\rho(1/r^2)$. If we assume that the beam is uniformly distributed over an area πr_o^2, where $4/3\,\pi r_o^3 = .05\ cm^3$ is the volume of the excitation region in the experiment of Hill, Heybey, and Walters, then the distribution function for r is

$$\rho(r) = \frac{2r}{r_o^2} \quad \text{for } r_o \geq r \geq 0$$

$$= 0 \quad \text{for } r > r_o$$

Since distribution functions are related by

$$\rho(f(r))\,df = \rho(r)\,dr,$$

$$\overline{\frac{1}{r^2}} = \int_o^{r_o} \frac{1}{r^2}\,\frac{2r}{r_o^2}\,dr = \frac{2}{r_o^2}\,\ln r\Big|_o^{r_o}.$$

The singularity at r = 0 is removed by assuming that a beam electron will not come within 1Å of a metastable spin. Then

$$\overline{\frac{1}{r^2}} = \frac{2}{r_o^2}\,(\ln r_o - \ln 1\text{Å}) \quad \text{and}$$

$$W = 4 \times 10^{-30}\frac{I}{e}\,\frac{2}{r_o^2}\,(\ln r_o - \ln 1\text{Å}) = 1.6 \times 10^{-10}\,s^{-1}.$$

$$T_1 = 3.1 \times 10^9\,s$$

This process of relaxation is thus much too slow.

To calculate the relaxation time due to the spin-spin interaction with the free electrons present in the excitation region, we shall use $T_1 = \frac{40\pi dD}{\mu_o^2 N \gamma^4 \hbar^2}$ where d is the

distance of closest approach, D is the diffusion coefficient of electrons in liquid helium, and N is the concentration of electrons.[25] This expression was derived for an interaction

$$\mathcal{H}_1(t) = \frac{1}{2}\sum_{i,j=1}^{N} \frac{\bar{\sigma}_i \cdot \bar{\sigma}_j}{r_{ij}^3} - 3\frac{(\bar{\sigma}_i \cdot \bar{r}_{ij})(\bar{\sigma}_j \cdot \bar{r}_{ij})}{r_{ij}^5} ,$$

which varies with time according to the random motions of the spins $\bar{\sigma}_i$ in the liquid. The diffusion coefficient may be calculated from the classical expression[26]

$$D = \frac{kT}{6\pi a\eta}$$

for a sphere of radius a in a liquid of viscosity η.[27] Assuming that electrons and metastable molecules both move in bubbles of radius a, then d = 2a and at T = 1.5°K,

$$T_1 = \frac{1.21 \times 10^{13}}{N} \text{ s} .$$

Alternatively, we may use Einstein's relation[28] between mobility[29] and diffusion constant,

$$D = kTB,$$

and then

$$T_1 = \frac{1.31 \times 10^{13}}{N} \text{ s} .$$

To calculate the electron density N we assume that the beam injects $\frac{I}{e}$ electrons per second at one point into the liquid.

According to the diffusion equation

$$\frac{\partial \rho}{\partial t} = D\Delta\rho ,$$

the probability ρ of an electron injected at time t = 0, r = 0 being a distance r away at time t is

$$\rho(r,t) = (4\pi Dt)^{-3/2}\exp\left(-\frac{r^2}{4Dt}\right) .$$

However, it may be shown that the electrostatic repulsion of the electrons will cause the space charge to diffuse faster than this. Assuming that the electrons move radially in all directions from the point of injection, the number of electrons which pass through a sphere of radius r in a time dt must equal the number of electrons injected at the center of the sphere.

$$4\pi r^2 N(r)\, v(r)\, dt = \frac{I}{e}\, dt$$

The velocity v(r) is determined by the mobility B and space charge field E.

$$v(r) = BeE(r)$$

Gauss's law relates the field E to the charge density eN.

$$\bar{\nabla}\cdot\bar{E}(r) = \frac{e}{\epsilon_o} N(r) .$$

Combining these equations we obtain

$$4\pi r^2 \frac{dE}{dr}\frac{\epsilon_o}{e} BeE = \frac{I}{e}$$

$$E = \sqrt{\frac{I}{2\pi r Be\epsilon_o}}$$

$$N(r) = \sqrt{\frac{I\epsilon_o}{\pi B}} \quad \frac{1}{(2er)^{3/2}}$$

The average charge density is

$$N = \left(\frac{4}{3}\pi r_o^3\right)^{-1} \int_0^{r_o} N(r)\, 4\pi r^2 dr = \frac{1}{(r_o e)^{3/2}} \sqrt{\frac{I\epsilon_o}{2\pi B}}$$

For $I = 1\mu A$ and $B = 1.7 \times 10^{14}$ m/sec-Newton[29],

$$N = 1.3 \times 10^{10} \text{ electrons/cm}^3.$$

Thus the relaxation time due to interaction with the free electrons is approximately

$$T_1 = 10^3 \text{ s},$$

making this mechanism ineffective at relaxing the metastable spin system. This result was referred to on p. 33.

(In this calculation of the electron density, the low-field value of mobility was used. The mobility of ions has been found[30] to be approximately constant until the energy of the electrons reaches a critical value. Above this value, the mobility sharply decreases with increasing electric field. It might therefore be asked if the mobility of the electrons is not much smaller at the center of the excitation region, where the space charge field is largest. The critical field E_c may be calculated using a theory of Huang and Olinto.[31]

$$E_c = 304 \exp 8.65^\circ \left(\frac{1}{.889^\circ} - \frac{1}{T}\right) \text{V/cm} = 16{,}000 \text{ V/cm for } 1.5^\circ\text{K}$$

Using our formula for the space charge field, the region in which the critical field is exceeded is found to be a sphere of radius

$$r = \frac{I}{2\pi B e \epsilon_0 E_c^2} = .0258 \text{ cm} .$$

This volume is x700 less than the .05 cm^3 excitation region and was assumed to have little effect on the average charge density.)

The last relaxation mechanism in liquid ^4He to be considered is the metastable-metastable interaction. Using the formulas

$$T_1 = \frac{40\pi dD}{\mu_0^2 N \gamma^4 \hbar^2} \quad \text{and}$$

$$D = \frac{kT}{6\pi a \eta}$$

we find for T = 1.5° , η = 13.5μP, N = $10^{13} cm^{-3}$, and a bubble radius a = $\frac{1}{2}$ d that

$$T_1 = 1.21 \text{ s} .$$

This means that the metastable spins are not relaxed by metastable-metastable interactions during their 7 x 10^{-4}s lifetime.

Since none of the interactions present in liquid ^4He relax the $a^3\Sigma_u^+$ spins, to observe EPR of this species it is necessary to introduce other relaxation mechanisms. By mixing ^3He with the liquid ^4He, a hyperfine interaction, between the

^{3}He nuclear spin and the metastable electronic spin, is added. The relaxation time calculated by our liquid model is

$$T_1 = \frac{40\pi dD}{\mu_o^2 N \gamma_n^2 \gamma_e^2 \hbar^2}$$

$$= 1.21\text{s} \times \frac{\gamma_e^2}{\gamma_n^2} \times \frac{10^{13}\text{cm}^{-3}}{N}$$

$$= \frac{5.24 \times 10^{18}}{N} \text{ s}$$

For a 1:1 mixture of ^{3}He - ^{4}He, $N \sim 10^{22}\text{cm}^{-3}$, and

$$T_1 = 5 \times 10^{-4}\text{s}$$

The $a^3\Sigma_u^+$ spin system in a ^{3}He - ^{4}He mixture may therefore be relaxed within the metastable lifetime.

The transverse relaxation time T_2 is the time constant of the approach to equilibrium of the transverse components of magnetization.

$$\frac{dM_x}{dt} = -\frac{M_x}{T_2} \text{ and } \frac{dM_y}{dt} = -\frac{M_y}{T_2}$$

The two relaxation times T_1 and T_2 may be shown to be equal if the random variations in the interaction $\mathcal{H}_1(t)$ are much more rapid than the Larmor precession. This situation, known as "extreme narrowing", is defined by the condition $\tau\omega_o \ll 1$ where τ is the correlation time of $\mathcal{H}_1(t)$ and ω_o is the Larmor frequency. If we take τ to be the time between

collisions, we may estimate it by treating liquid helium like a dense gas. Then the time between ^4He - He_2^m collisions may be calculated to be 10^{-14}s, and since the Larmor frequency is 10^{10}Hz, this condition is satisfied and $T_1 = T_2$.

Having calculated both relaxation times and determined the effect of the finite lifetime of the metastable molecules, we may calculate the minimum detectable number of metastable spins. The saturation factor

$$1 + \frac{\gamma^2 P T_1 T_2}{a} + \frac{T_1}{\tau}$$

will be appreciably larger than 1 for powers

$$P \geq \frac{a}{\gamma^2 T_1 T_2} = \frac{5 \times 10^7 W T^{-2}}{(1.76 \times 10^{11} s^{-1} T^{-1} \times 5 \times 10^{-4} s)^2} = 6.5 \times 10^{-9} W.$$

For this power the spectrometer sensitivity is

$$N_{min} = 6.7 \times 10^{12} \times \sqrt{\frac{10^{-4} W}{6.5 \times 10^{-9} W}} \simeq 10^{15} \text{ spins.}$$

This result is referred to on p. 34.

Symbols

Roman symbols	First used on page
A = Ampere = MKS unit of current	7
$\mathring{A}$ = Ångstron = 10^{-8}cm = unit of length	50
$A = \frac{1}{8} E\gamma Q_u \chi_o \omega_o Z$	59
AM = amplitude modulated	27
a = power absorbed in cavity walls for unit microwave magnetic induction B_1	63
a = radius of sphere diffusing through superfluid helium	72
B = Bel = unit of logarithm_{10} of ratio of powers	22
B = magnetic induction	55
B_o = static 3kG magnetic induction	57
ΔB_{pp} = peak-to-peak width of first derivative of EPR absorption line	57
B_m = modulation magnetic induction	59
$B = B_m / \Delta B_{pp}$	60
B_{max} = value of modulation field that maximizes EPR line height	61
B_{broad} = maximum modulation field without line broadening	61
B_1 = microwave magnetic induction	63
B = mobility of an ion in superfluid helium	72
$b = \gamma^2/a$	63
C = correction factor to minimum detectable number of spins	61

$g(B) = g(\omega)$ = absorption line shape function, dependence of microwave power absorbed on magnetic field or frequency 59

H = magnetic field 55

H_o = static 3kOe magnetic field 55

H_1 = microwave magnetic field 55

HV = high voltage 7

$\mathcal{H}_o$ = Hamiltonian of interaction between a single electronic spin and a static magnetic field H_o 66

$\mathcal{H}_1$ = Hamiltonian of interaction between a single electronic spin and a perturbing microwave field H_1 66

Hz = Hertz = unit of frequency 2

$\hbar$ = Planck's constant $\div 2 = 1.054 \times 10^{-34}$ J-s 66

hr = hour = unit of time 10

I = electron beam current 71

ID = inner dimension 14

IR = infrared 2

$i = \sqrt{-1}$

i = summation index 70

i.f. = intermediate frequency, between microwave frequency and modulation frequency 59

i-v = current v.s. voltage 25

J = Joule = MKS unit of energy

j = summation index 72

°K = degree Kelvin = unit of temperature 2

k = kilo = 10^3 1

k = Boltzmann's constant = $1.38 \times 10^{-23} J/^{o}K$	28
L = equivalent inductance of cavity	53
M = mega = 10^{6}	36
M = magnetization	56
M_o = value of M at thermal equilibrium	65
m = milli = 10^{-3}	
m = meter = MKS unit of length	19
m_s = magnetic quantum number	33
mho = MKS unit of conductance	19
min = minutes = unit of time	51
N = number of free elctrons per m^3	71
N_o = noise power at output	28
N_i = noise power at input	28
N_{min} = minimum detectable number of spins	28
N_+ = population of electrons in $\|+\rangle$ state	67
n = nano = 10^{-9}	10
n = excess population in $\|+\rangle$ state = $N_+ - N_-$	68
n_o = value of n at thermal equilibrium for $\tau = \infty$ and $B_1 = 0$	68
n_s = value of n for $\tau < \infty$ and $B_1 > 0$	68
OD = outer dimension	14
Oe = Oersted = CGS unit of magnetic field	
P = probability per second of a transition stimulated by the perturbing field B_1	67
P_w = power incident on cavity	56

Q = quality factor (see also p. 55) 19

Q_u = unloaded cavity quality factor, due to losses through iris and in walls 55

Q_χ = cavity quality factor due to losses in sample 55

R = equivalent resistance of cavity and sample 53

R_g = equivalent resistance of waveguide above cavity 56

r_o = radius of spherical region in which metastable helium states exist in superfluid helium bombarded by electrons 71

r.f. = radio frequency (microwaves here) 34

S_i = signal power at input 29

S/N = ratio of signal power to noise power 54

s = second = unit of time 33

T = temperature

T_1 = longitudinal relaxation time 34

T_2 = transverse relaxation time 34

T_s = sample and cavity temperature 28

T_e = electron spin temperature 29

T = Tesla = MKS unit of magnetic induction 77

t = time

V = Volt = MKS unit of electric potential 7

V_s = sample volume 57

V_c = cavity volume 57

v = volume 55

v = velocity of beam electrons 70

v = velocity of diffusing space charge 73

W = average transition probability per second between spin states = $\frac{1}{2}(W_+ + W_-)$ 65

W = Watt = MKS unit of power 24

W = work 55

$W = \frac{\omega_o - \omega}{\Delta\omega_{pp}}$ 60

W_+ = probability per second of a transition from $|+\rangle$ to $|-\rangle$ 67

W_- = probability per second of a transition from $|-\rangle$ to $|+\rangle$ 67

w = probability per second of a spin flip induced by a single beam electron 70

X = rate of production of metastable states 67

X-band = set of frequencies from 8.2GHz to 12.4GHz 20

$\hat{x}$ = vertical unit vector up, parallel to microwave magnetic field at the sample 56

Z = saturation factor = $(1 + \frac{1}{2}\gamma^2 B_1^2 T_1 g(\omega))^{-1}$ 59

$\hat{z}$ = horizontal unit vector in direction of electron beam

Z_g = impedance of waveguide above cavity 54

Z_1 = impedance of cavity and sample 54

Greek symbols

β = Bohr magneton = 9.28×10^{-24} J/T 57

γ or γ_e = electronic gyromagnetic ratio = 1.76×10^{11} $s^{-1}T^{-1}$ 60

γ_n = nuclear gyromagnetic ratio = 2.675×10^{8} $s^{-1}T^{-1}$ 76

Δ = change in the quantity whose symbol follows

ϵ_o = permittivity of a vacuum = $10^7/4\ c^2$ MKS units

η = viscosity 72

η = filling factor 56

θ = polar coordinate

μ = micro = 10^{-6} 9

μ_o = permeability of a vacuum = 4×10^{-7} MKS units 56

π = 3.14159...

ρ = distribution function 70

σ = electron spin magnetic moment 65

τ = lifetime of metastable state 67

τ = correlation time of random perturbation $\mathcal{H}_1(t)$ 76

χ_o = static susceptibility 56

χ' = in-phase rlfl susceptibility 56

χ'' = out-of-phase r.f. susceptibility 56

ω = angular frequency = $2\pi f$

ω_o = cavity resonant frequency 55

ω_o = EPR frequency 55

$\Delta\omega_{pp}$ = peak-to-peak width of first derivative of EPR absorption line 60

Other symbols

$[H]$ = concentration of H atoms in moles/cc 40

$|+\rangle$ = state ket for $m_s = +1/2$ 65

$|\sigma(t)\rangle$ = time-dependent electron spin ket 65

References

		Page
1.	J. Jortner, L. Meyer, S. A. Rice, and E. G. Wilson, "Energy Transfer Phenomena in Liquid Helium," Phys. Rev. Letters 12, 15, 415 (1964).	2
2.	Wiley Sam Dennis, Electron Beam Excitation Studies of Helium, M. A. Thesis, Rice University (1967).	2, 18, 30
3.	Edgar Durbin Jr., Spectra of Dense Helium Excited by Electron Impact, M. A. Thesis, Rice University (1969).	2, 18, 31
4.	Wiley Sam Dennis, Optical and Infrared Emission Spectra of Electron-bombarded Liquid Helium, Ph.D. Thesis, Rice University (1969).	2, 31
5.	W. S. Dennis, E. Durbin Jr., W. A. Fitzsimmons, O. Heybey, G. K. Walters, "Spectroscopic Identification of Excited Atomic and Molecular States in Electron-bombarded Liquid Helium," Phys. Rev. Letters 23, 1083 (1969).	2, 30
6.	J. C. Hill, O. Heybey, and G. K. Walters, "Evidence of Metastable Atomic and Molecular Bubble States in Electron-bombarded Superfluid Liquid Helium," Phys. Rev. Letters 26, 1213 (1971).	3, 32, 69
7.	L. H. Piette, R. C. Rempel, H. E. Weaver, J. M. Flournoy, "EPR Studies of Electron Irradiated Ice and Solid Hydrogen," J. Chem. Phys. 30, 1623 (1959).	3, 36
8.	K. H. Steigerwald, "Ein neuartiges Strahlerzeugungs-System für Elektronenmikroskope," Optik 5, 469 (1949).	7
9.	F. W. Braucks, "Untersuchungen an der Fernfokuskathode nach Steigerwald," Optik 15, 242 (1958).	7
10.	P. Grivet, Electron Optics, Pergamon Press, 1965, p. 450.	9

11. Russell O. Wright, "The Backward Diode--When and How To Use It," Microwaves, December 1964. 26

12. A. P. Hickman and N. F. Lane, "Localized Excited States of Helium in Liquid Helium," Phys. Rev. Letters 26, 1216 (1971). 31

13. Bell Telephone Laboratories, Index to the Literature of Magnetism. 32

14. B. H. J. Bielski, and J. M. Gebicki, Atlas of EPR Spectra, Academic Press, 1967. (Up to late 1964). 32

15. H. M. Hershenson, Nuclear Magnetic Resonance and ESR Spectra Index for 1958-63, Academic Press, 1965. 32

16. J. E. Bennett and D. R. Blackmore, "Gas-phase Recombination Rates of Hydrogen and Deuterium Atoms," J. Chem. Phys. 53, 4400 (1970). 40

17. Sir James Jeans, The Dynamical Theory of Gases, 4th edition, Dover, 1954, p. 37. 40

18. J. V. Davies, M. Ebert, and R. J. Shalek, "The Radiolysis of Dilute Solutions of Lysozyme. II Pulse Radiolysis Studies With Cysteine and Oxygen," Int. J. Radiat. Biol. 14, 19-27 (1968). 42, 50

19. Hermann Dertinger and Horst Jung, Molecular Radiation Biology, Springer-Verlag, 1970, p. 6. 45

20. R. J. Shalek, "Radiation Effects on Dilute Solutions of Lysozyme," Progress Report, N.C.I. Grant C-3283(C3), April 30, 1961. 49

21. G. Feher, "Sensitivity Considerations in Microwave Para-magnetic Resonance Absorption Techniques," Bell System Technical Journal,XXXVI, no. 2, 449 (1957). 53

22. C. P. Poole Jr., ESR; A Comprehensive Treatise on Experimental Techniques, John Wiley, New York, 1967, Chapter 14. 53

23. E. R. Andrew, Nuclear Magnetic Resonance, Cambridge University Press (1969), Chapter 2. 51, 60, 65

24. Julius Adams Stratton, Electromagnetic Theory, McGraw - Hill (1941), p. 232. 20

25. A. Abragam, The Principles of Nuclear Magnetism, Oxford (1961), p. 302. 72

26. Ibid., p. 300. 72

27. R. J. Donnelly, Experimental Superfluidity, University of Chicago (1967), p. 234. 72

28. D. K. C. MacDonald, Noise and Fluctuations, John Wiley (1962), p. 22. 72

29. R. J. Donnelly, Op. cit., p. 243. 72

30. G. Careri, S. Consolo, P. Mazzoldi, and M. Santini, Proceedings of 9th Int. Conf. on Low Temp. Physics, J. G. Daunt, et al eds., Plenum (1965). 74

31. K. Huang and A. C. Olinto, "Quantized Vortex Rings in Superfluid Helium; A Phenomenological Theory," Phys. Rev. 139A, 1441 (1965). 74

Acknowledgements

The author is pleased to have this occasion to acknowledge the help he received from so many friends and colleagues in the work reported in this thesis. His principal guide and advisor in four years at Rice University has been King Walters. Advice has also been generously given by other faculty members, including Steve Baker, Paul Donoho, Robert J. Shalek, Thomas Estle, and Ronald Stebbings. A great part of the design of the apparatus was contributed by the research associates involved in this project, Bill Fitzsimmons, Mike McCusker, and Ot Heybey. Construction of the elements of the apparatus was accomplished principally by Ed Surles, Bill O'Rear, Piet DeVries, Don Hardy, and Jim Godwin; and these men also served as the author's instructors in the arts and sciences of the shop. The largest group of collaborators in this work is the graduate students of the Rice Physics Department. Wiley Dennis, Arlen Barksdale, Walter Steets, Wilber Boykin, Jim McCarty, Tom B. Cook, Jim Herrington, Clif Hill, Paul Keliher, A. C. Conrad, George Bakken, Don Pederson, Roland Schreiber, Brahm Bhardwaj, Carey Snyder, L. V. Benningfield, Norman Gabitsch, Jess Carnes, Bob Timme, Lewis Shen, Tim Casey, and Charley Wells all contributed something specific; and this list is not complete. Financial

support for the author was provided by the Atomic Energy Commission, Rice University, and the Veterans Administration, represented respectively by King Walters, by H. R. Rorschach, and by W. B. Bandy and C. M. Neumann. This thesis was typed by Libby Potter, who also, by her questions and interest in the work, provided the occasion for the author to first formulate in his own mind explanations included here.

The committee that discussed this thesis with the author included King Walters, George Trammell, and Graham Glass.